Elsevier Editorial System(tm) for Acta Biomaterialia

Manuscript Draft

Manuscript Number: AB-17-2249R2

Title: Heparin functionalization increases retention of TGF-β2 and GDF5 on biphasic silk fibroin scaffolds for tendon/ligament-to-bone tissue engineering

Article Type: Full length article

Keywords: Enthesis, Heparin, Transforming growth factor β2, Growth/differentiation factor 5, Silk fibroin, Tissue engineering

Corresponding Author: Dr. Elizabeth R. Balmayor, Ph.D.

Corresponding Author's Institution: Technical University of Munich

First Author: Sònia Font Tellado, M.Sc

Order of Authors: Sònia Font Tellado, M.Sc; Silvia Chiera; Walter Bonani; Patrina S. P. Poh, PhD; Claudio Migliaresi; Antonella Motta; Elizabeth R. Balmayor; Martijn van Griensven

Abstract: The tendon/ligament-to-bone transition (enthesis) is a highly specialized interface tissue with structural gradients of extracellular matrix composition, collagen molecule alignment and mineralization. These structural features are essential for enthesis function, but are often not regenerated after injury. Tissue engineering is a promising strategy for enthesis repair. Engineering of complex tissue interfaces such as the enthesis is likely to require a combination of biophysical, biological and chemical cues to achieve functional tissue regeneration. In this study, we cultured human primary adipose-derived mesenchymal stem cells (AdMCs) on biphasic silk fibroin scaffolds with integrated anisotropic (tendon/ligament-like) and isotropic (bone/cartilage like) pore alignment. We functionalized those scaffolds with heparin and explored their ability to deliver transforming growth factor β2 (TGF-β2) and growth/differentiation factor 5 (GDF5). Heparin functionalization increased the amount of TGF-β2 and GDF5 remaining attached to the scaffold matrix and resulted in biological effects at low growth factor doses. We analyzed the combined impact of pore alignment and growth factors on AdMSCs. TGF-β2 and pore anisotropy synergistically increased the expression of tendon/ligament markers and collagen I protein content. In addition, the combined delivery of TGF-β2 and GDF5 enhanced the expression of cartilage markers and collagen II protein content on substrates with isotropic porosity, whereas enthesis markers were enhanced in areas of mixed anisotropic/isotropic porosity. Altogether, the data obtained in this study improves current understanding on the combined effects of biological and structural cues on stem cell fate and presents a promising strategy for tendon/ligament-to-bone regeneration.

Klinikum rechts der Isar – UC – 81664 Munich, Germany

Professor William R. Wagner, Ph.D., FBSE
Editor-in-Chief
Acta Biomaterialia

Klinikum rechts der Isar
Public Agency

Experimental Trauma Surgery
Director:
Martijn van Griensven, MD, PhD

Department of Trauma Surgery
Supraregional Trauma Center
Accident Insurance Consultancy
Approved for VAV, SAV

Elizabeth Rosado Balmayor, PhD
Assistant Professor
Junior Group Leader

Ismaninger Strasse 22
81675 Munich, Germany
www.unfallchirurgie.mri.tum.de
Email:
Elizabeth.Rosado-Balmayor@tum.de
Tel: +49 (0)89 41 40 – 97 54
Fax: +49 (0)89 41 40 – 62 22

February 28, 2018

RE: Revision #2 for MS AB-17-2249

Dear Professor Wagner,

it is a great pleasure for me to submit the revised version (R2) of our manuscript entitled **"Heparin functionalization increases retention of TGF-β2 and GDF5 on biphasic silk fibroin scaffolds for tendon/ligament-to-bone tissue engineering"** for your consideration for publication in *Acta Biomaterialia.*

We would like to thank you very much for considering our study for publication in *Acta Biomaterialia*. We are very grateful for the opportunity given to our manuscript.

According to the minor change suggested by reviewer #1, we have changed the subtitles in the results section briefing the relevant findings and conclusions of our study. In addition, we have corrected the subheading numbers in the result section, as one number was repeated. Moreover, the word "AdMSC" and gene names have been written in a uniform manner throughout the text.

Together with the new MS file, we are submitting a document, signed by all authors that confirms that everyone agrees to the addition and order on the new co-author i.e. Patrina S.P. Poh, PhD, as well as the change in corresponding author.

We would like to thank you again for this great opportunity given to our study by you and the reviewers.

Thank you in advance for your consideration.

Yours truly,

Elizabeth Rosado Balmayor, PhD
On behalf of all authors
Assistant Prof. Experimental Trauma Surgery
Junior Group Leader

Statement Authorship

TraumaLab

Klinikum rechts der Isar

Technische Universität München

Klinikum rechts der Isar – UC – 81664 Munich, Germany
William R. Wagner, Ph.D., FBSE
Editor-in-Chief
Acta Biomaterialia

50 JAHRE UNIVERSITÄTS KLINIKUM RECHTS DER ISAR

DIE DEUTSCHEN UNIVERSITÄTSKLINIKA®
Klinikum rechts der Isar
Public Agency

Experimental Trauma Surgery
Director:
Martijn van Griensven, MD, PhD

Department of Trauma Surgery
SAV
Supraregional Trauma Center
Accident Insurance Consultancy
Approved for VAV, SAV

Martijn van Griensven, MD, PhD
Director

Ismaninger Strasse 22
81675 Munich, Germany
www.unfallchirurgie.mri.tum.de
Email:
Martijn.vanGriensven@tum.de
Tel: +49 (0)89 41 40 – 69 35
Fax: +49 (0)89 41 40 – 75 26

Munich, February 19 2018

RE: AB-17-2249R1, new co-author

Dear Prof. Wagner,

Thank you for the positive email regarding our above mentioned manuscript. This letter is a confirmation of all authors that everyone agrees to addition and order of the new co-author Patrina S.P. Poh, as well as the change in corresponding author to Elizabeth Rosado Balmayor.

Yours truly,

Elizabeth R. Balmayor

Sònia Font Tellado

Silvia Chiera

Walter Bonani

Patrina S. P. Poh

Claudio Migliaresi

Antonella Motta

Martijn van Griensven

Heparin functionalization increases retention of TGF-β2 and GDF5 on biphasic silk fibroin scaffolds for tendon/ligament-to-bone tissue engineering

Sònia Font Tellado[a], Silvia Chiera[b], Walter Bonani[b,c], Patrina S.P. Poh[a], Claudio Migliaresi[b,c], Antonella Motta[b], Elizabeth R. Balmayor[a]*, Martijn van Griensven[a]

a. Department of Experimental Trauma Surgery, Klinikum rechts der Isar, Technical University of Munich, Munich, Germany

b. BIOtech Research Center and European Institute of Excellence on Tissue Engineering and Regenerative Medicine, Department of Industrial Engineering, University of Trento, Trento, Italy

c. INSTM - National Interuniversity Consortium of Materials Science and Technology, Trento Research Unit, Trento, Italy

Contact information:

Sònia Font Tellado: sonia.font@tum.de
Silvia Chiera: silvia.chiera.1@unitn.it
Walter Bonani: walter.bonani@unitn.it
Patrina S.P. Poh: Patrina.poh@tum.de
Claudio Migliaresi: claudio.migliaresi@unitn.it
Antonella Motta: antonella.motta@unitn.it
Elizabeth Rosado Balmayor: elizabeth.rosado-balmayor@tum.de
Martijn van Griensven: martijn.vangriensven@tum.de

***Corresponding autor:**
Elizabeth Rosado Balmayor, PhD
Assistant Professor for Experimental Trauma Surgery
Department of Experimental Trauma Surgery
Klinikum rechts der Isar
Technical University of Munich
Ismaningerstr 22
81675 Munich, Germany
Phone: +49-89-4140-9754
Fax: +49-89-4140-7526
e-mail: Elizabeth.Rosado-Balmayor@tum.de

Abstract

The tendon/ligament-to-bone transition (enthesis) is a highly specialized interface tissue with structural gradients of extracellular matrix composition, collagen molecule alignment and mineralization. These structural features are essential for enthesis function, but are often not regenerated after injury. Tissue engineering is a promising strategy for enthesis repair. Engineering of complex tissue interfaces such as the enthesis is likely to require a combination of biophysical, biological and chemical cues to achieve functional tissue regeneration. In this study, we cultured human primary adipose-derived mesenchymal stem cells (AdMCs) on biphasic silk fibroin scaffolds with integrated anisotropic (tendon/ligament-like) and isotropic (bone/cartilage like) pore alignment. We functionalized those scaffolds with heparin and explored their ability to deliver transforming growth factor β2 (TGF-β2) and growth/differentiation factor 5 (GDF5). Heparin functionalization increased the amount of TGF-β2 and GDF5 remaining attached to the scaffold matrix and resulted in biological effects at low growth factor doses. We analyzed the combined impact of pore alignment and growth factors on AdMSCs. TGF-β2 and pore anisotropy synergistically increased the expression of tendon/ligament markers and collagen I protein content. In addition, the combined delivery of TGF-β2 and GDF5 enhanced the expression of cartilage markers and collagen II protein content on substrates with isotropic porosity, whereas enthesis markers were enhanced in areas of mixed anisotropic/isotropic porosity. Altogether, the data obtained in this study improves current understanding on the combined effects of biological and structural cues on stem cell fate and presents a promising strategy for tendon/ligament-to-bone regeneration.

Keywords

Enthesis, Heparin, Transforming growth factor β2, Growth/differentiation factor 5, Silk fibroin, Tissue engineering

1. Introduction

The tendon/ligament-to-bone interface (enthesis) is a highly heterogeneous and specialized transition tissue that integrates tendons and ligaments with bones and stabilizes joints facilitating motion. Fibrocartilaginous entheses consist of 4 regions: tendon/ligament, non-mineralized fibrocartilage, mineralized fibrocartilage and bone [1, 2]. Extracellular matrix (ECM) composition and cell type are specific for each region. Tendons and ligaments are composed of highly aligned collagen I fibers and populated by elongated fibroblasts. Due to the high alignment of the collagen fibers, tendons and ligaments are mechanically anisotropic. Enthesis fibrocartilage is rich in collagen type II, collagen type III and proteoglycans, and is populated by round fibrochondrocytes. Bone is composed of oriented collagen I fibers, which are more isotropic compared to tendons and ligaments. The mechanical properties of bone are dominated by its mineral phase. Bone tissue is populated by osteoblasts, osteocytes and osteoclasts. Of note, collagen molecule alignment increases gradually towards the tendon/ligament zone, whereas mineral content increases gradually towards the bone zone [2]. These structural and ECM composition gradients result in progressive changes of mechanical properties that enable a smooth transfer of mechanical stresses from tendons/ligaments to bone. However, the structure of the enthesis is often not regenerated after injury, resulting in increased re-rupture rates and compromising long term tissue functionality and clinical outcome [1].

Tissue engineering is an attractive strategy for enthesis regeneration. Given the tight relationship between enthesis structure and function, tissue engineering strategies will benefit from scaffolds mimicking native structural features [1, 3]. Topographical cues such as the morphology, size and alignment of scaffold pores or fibers have been shown to significantly influence mechanical properties and cell behavior in bone, cartilage, tendon, and ligament tissue engineering studies [4, 5]. However, the effects of topographical cues on enthesis

regeneration have been less characterized. Recently, we fabricated biphasic silk fibroin scaffolds with anisotropic porosity at the tendon/ligament part, isotropic porosity at the bone part and mixed porosity at the transition that mimic the change in collagen molecule alignment along the native enthesis [6]. Silk fibroin is a highly biocompatible natural polymer. In its native state, the mechanical properties of silk fibers are close to those of human ligaments and tendons [6, 7]. We previously showed that pore morphology and alignment of biphasic silk fibroin scaffolds significantly influenced the cytoskeletal alignment and gene expression of human adipose-derived mesenchymal stem cells (AdMSCs) [6].

Although topographical cues play a key role in scaffold properties and cell responses, engineering of complex tissues such as the enthesis is likely to require further stimuli in the form of chemical and/or mechanical cues to achieve functional tissue regeneration [1, 8]. Growth factors are potent molecules to regulate stem cell behavior. However, growth factor therapies have been limited by the short half-lives of growth factors [9]. Safety and cost-effectiveness concerns result from the burst release kinetics of growth factors when administrated without optimal delivery systems. [10]. Thus, it is necessary to develop new strategies to keep growth factors local and increase their stability and/or biological activity with the objective to lower the doses needed to obtain biological effects.

In vivo growth factors are stored in the ECM, where they are protected from degradation and released upon need. In tissue engineering approaches, scaffolds can be used as a growth factor *reservoir* to keep growth factors local and protect them from degradation [8, 11]. The sulfated glycosaminoglycan (GAG) heparin can be incorporated to scaffolds to improve growth factor retention on scaffold matrices. Heparin has been FDA approved for clinical use [10, 12] and can bind growth factors electrostatically, protecting them from enzymatic degradation and controlling their availability and local concentration [9, 13, 14]. In addition, binding to heparin can maintain and even increase the biological activity of growth factors [15-18]. This

represents an advantage compared to direct covalent binding of growth factors to scaffold matrices, in which protein activity can be compromised [12, 19]. In previous studies, heparin-based delivery systems have achieved sustained release of BMP-2 [20, 21], FGF-2 [10, 15], VEGF [22, 23], TGF-β1 [24], GDF5 [25] and platelet-derived growth factor (PDGF) [26].

Growth factors from the TGF-β family play key roles in musculoskeletal development and homeostasis. In particular, TGF-β1 and TGF-β3 are well established chondrogenic inductors [27, 28]. On the other hand, the effects of TGF-β growth factors on the differentiation of mesenchymal stem cells towards tendon/ligament fibroblasts and enthesis fibrochondrocytes are less understood. In this study, we focus on two TGF-β family growth factors containing heparin-binding domains: TGF-β2 and GDF5. TGF-β2 is required for fetal tendon development in mice [29] and has been shown to induce scleraxis (scx) expression in mouse [29] and chick [30] embryos. GDF5 has been shown to be important for the formation of bone, cartilage, ligaments and tendons [31]. Interestingly, some studies report that treatment with GDF5 increases GAG and collagen II production from chondrocytes without increasing that of collagen X, a marker for cartilage hypertrophy [32]. In addition, GDF5 has been suggested to play an important role during enthesis development [33]. Despite that, the effects of TGF-β2 and GDF5 in *in vitro* differentiation protocols for musculoskeletal tissue engineering have been under-studied in comparison to other TGF-β family members such as TGF-β1/3.

The main aims of this study were 1) to functionalize biphasic silk fibroin scaffolds with heparin to improve their bioactivity and capacity to retain growth factors, 2) to characterize the incorporation and release kinetics of TGF-β2 and GDF5 in heparin-functionalized vs. non-functionalized scaffolds, 3) to analyze the combined impact of chemical (growth factors) and biophysical (pore alignment) cues on AdMSCs gene expression and 4) to identify relevant cues able to selectively enhance specific tenogenic/ligamentogenic, fibrochondrogenic and

chondrogenic differentiation pathways for tendon/ligament-to-bone interface tissue engineering.

2. Materials and methods

All materials were purchased from Sigma-Aldrich (USA) unless otherwise stated.

2.1 Fabrication of biphasic silk fibroin scaffolds

Silk fibroin processing and scaffold fabrication were performed as described in [6]. Biphasic scaffolds with anisotropic and isotropic pores were fabricated using 8% silk fibroin solution following a two-step protocol [6]. In the first step, the isotropic part of the scaffold was produced by solvent casting/particulate leaching using NaCl salt crystals (400-800µm) as porogen. Disc-shaped scaffolds of 8mm diameter and 1.5mm thickness were obtained. In the second step, isotropic scaffolds were placed at the bottom of an 8mm polypropylene (PP) cylinder and covered with 800µl of 8% fibroin solution. The PP cylinder was tightly inserted in a cylindrical polystyrene foam mold, covering only the lateral surface of the cylinder, and placed at -20°C for 24h. The polystyrene mold acted as a heat insulator along the lateral surface of the cylinder, exposing only the free surface of the fibroin solution. This induced the formation of vertically oriented ice crystals by directional freezing along the main axis of the cylinder. Finally, the frozen scaffolds were lyophilized in an Alpha 1–2 LDplus freeze-dryer (Martin Christ, Germany) for 48h. Biphasic scaffolds (8mm diameter x 10mm length) with integrated anisotropic and isotropic porosities were obtained. Scaffolds were punched to a final dimension of 4mm diameter x 8mm length using biopsy punches (Stiefel, USA) and sterilized with 70% ethanol.

2.2 Characterization of biphasic silk fibroin scaffolds

The structure, pore morphology and pore alignment of biphasic silk fibroin scaffolds were characterized by observational light microscopy (VHX-900F, Keyence, Japan), micro-computed tomography (µCT) (Skyscan1176, Bruker, Belgium), scanning electron microscopy (SEM)

(Phenom Pro, LOT-Quantum Design, Germany) and fluorescent microscopy (BZ-9000, Keyence, Japan).

For μCT, scaffolds were scanned at 40kV with a voxel size of 9 μm. Image reconstruction was performed using NRecon (Version1.7.3; Bruker, Belgium). Scaffold characterization was performed using CTAn (Version 1.13, Bruker, Belgium). Firstly, three volumes of interest (VOI) were selected, representing the anisotropic (200 slices), transition (30 slices) and isotropic (60 slices) regions of the scaffold. Then, adaptive thresholding was implemented for the binarization of images. Finally, using CTAn built in algorithm for 3D structure analysis, the pore size distribution, porosity, fractal dimension (FD) and degree of anisotropic (DA) for each region was calculated (n= 6).

Scaffolds for light microscopy, SEM and fluorescent microscopy were cut in transversal sections of 1-1.5mm thickness using a scalpel. The characterization of the surface topography was performed in the VHX-900F microscope using a version 1.6.1.0 software and the VH-Z20R objective. Scaffolds used for SEM were coated with Pt/Pd alloy (80/20) using a Q150R sputter coater (LOT-Quantum Design, Germany). Scaffolds for fluorescence microscopy were stained with DAPI following the manufacturer's instructions.

2.3 Covalent binding of heparin to silk fibroin scaffolds

Heparin sodium salt from porcine intestinal mucosa was covalently attached to biphasic silk fibroin scaffolds after fabrication using carbodiimide chemistry. Prior to conjugation, silk fibroin scaffolds were incubated for 30 min in 0.1 M 2-(N-morpholino) ethanesulfonic acid (MES) buffer (pH 5.8). Next, heparin was dissolved in MES buffer at a concentration of 3% and sterile filtered using 0.20 μm filters (Sarstedt, Germany). 1-ethyl-3-(3-dimethylaminopropyl) carbodiimide hydrochloride (EDC) (Carl Roth, Germany) and N-hydroxysuccinimide (NHS) (Carl Roth, Germany) were added to the heparin solution at final concentrations of 0.25M and 0.125M, respectively, to activate carboxyl groups in heparin molecules. The reaction was

performed at room temperature (RT) for 15 min under shaking and quenched by adding 0.2M 2-mercaptoethanol. Subsequently, 1ml of heparin solution/scaffold was added to induce a covalent binding between activated carboxyl groups in heparin and primary amines in fibroin. The reaction was performed for 4h at RT under shaking. Scaffolds reacted with heparin in the presence of EDC/NHS are hereafter termed “scaffolds cross-linked with heparin”. In addition, 3% heparin solution was added to silk fibroin scaffolds in absence of EDC/NHS. Those scaffolds are hereafter termed “scaffolds non-cross-linked with heparin”. Untreated scaffolds will be termed “unmodified scaffolds”. After conjugation, all scaffolds were washed 5 times with MES buffer and 3 times with ddH_2O to remove unreacted heparin. Scaffolds used for growth factor incorporation and cell culture were additionally incubated for 3 days in ddH_2O under shaking to ensure complete removal of residual heparin (complete washing). Conjugation and washing were performed in sterile conditions.

2.4 Heparin conjugation efficiency and release

Heparin was quantified using a Blyscan Sulfated Glycosaminoglycan (GAG) assay (Bicolor, United Kingdom) following the instructions of the manufacturer. Binding efficiency of heparin to scaffolds (cross-linked vs. non-cross-linked) (n=6) was determined indirectly by measuring the amount of unbound heparin in MES buffer after the conjugation reaction (before washing). Unreacted 3% heparin solution was used as control of known concentration. Next, scaffolds were washed 5 times with 0.1M MES buffer and 3 times with ddH_2O. Subsequently, scaffolds were incubated in 1ml ddH_2O for quantification of heparin release. After 1h, 3h, 1d, 3d and 7d of incubation, 100µl of ddH_2O were taken for heparin quantification and replaced with 100µl fresh ddH_2O. To calculate the proportion of heparin remaining bound to scaffolds after complete washing, the amount of heparin released after 3 days in ddH_2O was subtracted from the total incorporated after conjugation.

2.5 TGF-β2 and GDF5 binding to silk fibroin scaffolds

Human recombinant TGF-β2 and GDF5 were purchased from PeproTech (USA). Silk fibroin scaffolds (unmodified, non-cross-linked with heparin and cross-linked with heparin) were loaded with TGF-β2, GDF5 or their combination. Growth factor loading was performed in whole scaffolds or in the anisotropic and isotropic parts separately. For growth factor loading on complete scaffolds, scaffolds of 4mm diameter x 8mm length were immersed in 500µl of a PBS solution containing 200ng/ml of TGF-β2 or GDF5 (single growth factor loading) or 100ng/ml of TGFβ2 and 100ng/ml of GDF5 (double growth factor loading). For growth factor loading on the anisotropic and isotropic parts separately, scaffolds were cut at the border between the two parts using a scalpel. Next, each scaffold part was incubated in a volume of growth factor solution proportional to its weight. The weight ratio between the anisotropic and isotropic parts was 2.5:1. Accordingly, the anisotropic part was incubated in 358µl of a PBS solution containing 200ng/ml of TGF-β2 or GDF5 (single growth factor loading). Similarly, a solution containing 100ng/ml of both growth factors, i.e. TGFβ2 and GDF5 was used for double growth factor loading. The isotropic part was incubated in 142µl of the same solutions. All scaffolds were incubated in the growth factor solution for 3h at RT while shaking.

2.6 Binding efficiency and release of TGF-β2 and GDF5

The efficiency of growth factor incorporation on scaffolds was evaluated indirectly by quantifying the amount of unbound growth factor in PBS after loading. TGF-β2 was quantified using a Human TGF-β2 ELISA kit (Diaclone, France) (n=3) and GDF5 using a GDF5 Quantikine ELISA kit (R&D, USA) (n=3) following the manufacturer's instructions. Analysis of cumulative growth factor release was performed by incubating the scaffolds (or individual scaffold parts) in 500µl DMEM containing 2% fetal calf serum (FCS) and 1% penicillin/streptomycin (P/S) at 37°C. Quantification was performed 1h, 3h, 1d, 3d, 7d and 14d after growth factor loading. 100µl of supernatant were removed, used for protein quantification and replenished with

100µl fresh medium at each measuring point. The amount of incorporated growth factor was expressed as percentage respect to the initial loading amount.

2.7 Adipose-derived mesenchymal stem cell (AdMSCs) isolation and expansion

Human adipose tissue was obtained from healthy donors (N=3) after written informed patient's consent. This study was approved by the Local Ethics Committee of the ''Klinikum Rechts der Isar'' at the Technical University of Munich, Germany. Isolation of AdMSCs from fat tissue was performed as reported in [34]. Briefly, fat tissue was cut in small pieces and placed in 15 ml PP tubes (Eppendorf, Germany). Next, the tissue was centrifuged at 430g to separate the stromal fraction. After centrifugation, fat tissue was digested with 1.45% collagenase solution (Merck Millipore, USA) for 30 min at 37°C and centrifuged at 600g to obtain a cell pellet. Cells were cultured in 175 cm^2 cell culture flasks (Eppendorf, Germany) in DMEM medium supplemented with 10% FCS and 1% P/S (AdMSCs growth medium). Cells were cultured at 37°C and 5% CO_2 in a humidified atmosphere. Medium was changed twice a week and cells were passaged when reaching 80% confluence.

2.8 AdMSCs culture on biphasic silk fibroin scaffolds

AdMSCs (passage 3) were seeded on biphasic silk fibroin scaffolds at a density of 4 x 10^5 cells/scaffold. To improve cell attachment, scaffolds were incubated in AdMSCs growth medium overnight before seeding. Cells were seeded on both scaffold sides (anisotropic and isotropic) in a volume of 60µl / scaffold (30µl on each side). Cells were left to attach for 2h at 37°C before replenishing with fresh medium. Culture medium was DMEM supplemented with 2% FCS and 1% P/S. Cells from 3 different donors were used for all experiments (N = 3).

2.9 Seeding efficiency and metabolic activity

AdMSCs metabolic activity and seeding efficiency on biphasic silk fibroin scaffolds was evaluated by 3-(4,5-Dimethylthiazol-2-yl)-2,5-diphenyltetrazoliumbromid (MTT) assay. AdMSCs

were cultured for 1, 3 or 7 days on unmodified scaffolds, scaffolds cross-linked with heparin without growth factors (unloaded) or scaffolds cross-linked with heparin and loaded with TGF-β2, GDF5 or their combination. After culture, scaffolds were washed with PBS and incubated for 2h in MTT solution (1.2 mM in PBS) (Roth). Blue precipitates formed as a consequence of cell metabolic activity. Next, the precipitates were dissolved by incubating the samples for 1h in isopropanol. Absorbance at 570 and 690nm was measured using a FLUOstar Omega photometer (Labtech, Germany). Seeding efficiency after 24h was calculated by determining the percentage of metabolically active cells on the scaffolds compared to the metabolic activity of total cells seeded. This was done by calculating the ratio between the OD of total cells seeded and the OD of cells attached to the scaffolds.

2.10 Gene expression

The gene expression of tendon/ligament markers (scx, collagen I, mohawk and tenascin C), cartilage markers (SRY-box 9 (sox9), collagen II and aggrecan) and enthesis markers (sox9, scx, collagen II, collagen III, tenascin C and aggrecan) were analyzed by quantitative polymerase chain reaction (qPCR). The primers used are shown in table 1. AdMSCs (N=3, n=9) were cultured for 7 or 14 days on biphasic silk fibroin scaffolds. Four groups were analyzed: scaffolds without growth factors (unloaded), scaffolds loaded with TGF-β2, scaffolds loaded with GDF5 and scaffolds loaded with TGF-β2 + GDF5 (all cross-linked with heparin). After culture, samples were washed with PBS and cut in 3 parts: anisotropic, transition and isotropic. The anisotropic and isotropic regions can be visually distinguished. The transition region was defined as the 1mm thick area around the border between the anisotropic and isotropic regions (0.5mm up and 0.5mm down the border). Scaffold pieces were stored at -80°C in TRIreagent for at least 24h. RNA isolation was performed by chloroform extraction in each of the 3 scaffold parts (anisotropic, transition and isotropic) separately. RNA quantification and quality control were done with NanoDrop (Nanodrop Tech, USA). Reverse transcription to cDNA was performed in a

C1000 Touch Thermal Cycler (Eppendorf, Germany) using a first strand cDNA synthesis kit (Thermo Scientific, USA) and following the instructions of the manufacturer. qPCR was performed in a CFX96 Real Time System thermocycler using Sso Fast EvaGreen supermix (BioRad, Hercules, CA, USA) as a detection reagent. Gene expression data from scaffolds loaded with growth factors was expressed as $2^{-\Delta\Delta CT}$ relative to the housekeeper (β-Tubulin) and to the scaffolds without growth factors (unloaded).

Table 1. Primers used for qPCR

Target	**Forward (5' → 3')**	Reverse (5' → 3')
Aggrecan	TCGAGGACAGCGAGGCC	TCGAGGGTGTAGCGTGTAGAGA
β-Tubulin	GAGGGCGAGGACGAGGCTTA	TCTAACAGAGGCAAAACTGAGCACC
Collagen I A1	AGCGGACGCTAACCCCCTCC	CAGACGGGACAGCACTCGCC
Collagen II	AACCAGATTGAGAGCATCCG	ACCTTCATGGCGTCCAAG
Collagen III	TACTTCTCGCTCTGCTTCATCC	GAACGGATCCTGAGTCACAGAC
Mohawk	TGGTTTGCTAATGCAAGACG	CCTTCGTTCATGTGGGTTCT
Scleraxis	CAGCCCAAACAGATCTGCACCTT	CTGTCTTTCTGTCGCGGTCCTT
Sox9	GAGCCGAAAGCGGAGCTGGAA	ACAGCTGCCCGCTCCAAGTG

2.11 Immunofluorescence and confocal microscopy

The presence of collagens type I, II and III in biphasic silk fibroin scaffolds was evaluated by immunofluorescence staining. The samples were imaged using a confocal microscope (Nikon A1, Nikon Instruments, The Netherlands). AdMSCs were cultured for 14 days on heparin-cross-linked biphasic silk fibroin scaffolds. Four groups were analyzed: scaffolds without growth factors (unloaded), scaffolds loaded with TGF-β2, scaffolds loaded with GDF5 and scaffolds loaded with TGF-β2 + GDF5 (all cross-linked with heparin). After 14 days of culture, samples

were washed 3 times with PBS at 37°C and fixed with 10% formalin solution for 40 min at RT. After fixation, samples were washed with PBS and blocked with 1% bovine serum albumin (BSA) solution in PBS for 1h at RT. Staining with primary antibodies (Abcam, Germany) for collagen I (ab34710, 1:500 in 1% BSA), collagen II (ab34712, 1:200 in 1% BSA) and collagen III (ab7778, 1:200 in 1% BSA) was performed overnight at 4°C. Next, samples were washed 3 times with PBS and incubated with secondary fluorescent antibody solution (Abcam ab150077, 1:1000 in PBS) for 1h at RT. Subsequently, samples were stained with DAPI and Alexa Fluor 594 Phalloidin (Thermo Fisher Scientific, USA) and stored in PBS until imaging. Semi-quantification of collagen expression was performed using ImageJ software (v1.50i, NIH, Bethesda, USA, https://imagej.nih.gov/ij). For this, three regions of interest (ROIs) were defined for each scaffold by manually defining the contours of each part, i.e. anisotropic, transition and isotropic using the freehand selection tool. Next, each ROI was analyzed using the color threshold function to identify areas of collagen positive staining (green) within the scaffold regions. The semi-quantification routine was performed for all the images under the same conditions (previously adjusted in the software). Six different scientists independently performed the selection of the ROIs and semi-quantification of all the images. Finally, the thresholded area (positive collagen expression) was divided by the total area to calculate the percentage.

2.12 Statistical analysis

Statistical analysis was performed using GraphPad Prism version 5.00 (GraphPad software, USA). Data was analyzed by One-way ANOVA and Tukey correction (more than two groups, Gaussian distribution), Kruskal-Wallis and Dunn's correction (more than two groups, non-Gaussian distribution) or Student's t-test (two groups, Gaussian distribution). Values were considered significant at $p<0.05$.

3. Results

3.1 Morphology and pore alignment of biphasic silk fibroin scaffolds recreates the bony and tendon/ligament part of the native enthesis

Biphasic silk fibroin scaffolds have a porous structure and cylindrical shape. Scaffold dimensions are 4 mm in diameter and 8 mm in length. The scaffolds are composed of two regions, i.e. anisotropic (tendon/ligament part) and isotropic (bony part) (figures 1A and 1B).

Macroscopic view of scaffold (figure 1A) show lamellar-like structure on the tendon/ligament part and trabecular-like structure on the bony part, with a smooth transition of the structures across the two regions. Further evaluation of the scaffolds' surface topography (Figure 1A, right upper corner) show relatively smoother surfaces on the bony part as compared to the tendon/ligament and transition regions. Three-dimensional evaluation of the scaffolds properties by µCT (figure 1B) revealed a fractal pattern of the scaffold structures (FD value between 2 to 3) and ellipsoidal pores throughout the entire construct. The tendon/ligament part comprised of larger pores compared to that of transition and bony part. This observation was in line with pore-size distribution between the three regions (figure 1C), whereby the bony part shows significantly higher proportion of pores > 500 µm compared to the transition and bony part (24.71% vs 7.98% and 9.48%). Analysis of DA indicated that the pores at the tendon/ligament part were better aligned the longitudinal plane compared to that of the transition and bony part. Similar pores structure was observed microscopically by SEM (figure 1D). Notably, porosity of scaffolds was maintained at ~65-70% across the structure with negligible close porosity, indicating highly interconnected pores.

3.2 Heparin was stably bound on the scaffolds' surface

Heparin incorporation in biphasic silk fibroin scaffolds was quantified as the percentage of heparin bound to the scaffolds with respect to the total amount supplemented for

conjugation. The efficiency of heparin incorporation in the scaffolds changed depending on the use of EDC/NHS cross-linkers during conjugation (figure 2A, patterned bars). In non-cross-linked scaffolds, the percentage of heparin bound to scaffolds after conjugation (before washing) was 6.0 ± 2.3%. Using EDC/NHS for scaffold functionalization, the percentage of bound heparin increased (before washing) to 29.5 ± 4.4% ($p<0.001$).

In order to evaluate the stability of the heparin incorporation, its cumulative release in ddH_2O was quantified over a period of 7 days. The amount of heparin released from the scaffolds was expressed as percentage relative to the total amount of heparin bound to the scaffolds after conjugation (figure 2B). In both, heparin cross-linked and non-cross-linked scaffolds, between 9-9.5% of total incorporated heparin was released over a period of 7 days. In absence of EDC/NHS, heparin release happened faster. In this case, 6% of incorporated heparin was released already after 24h. In the presence of cross-linkers, heparin release was more sustained with 3.5% being released 24h after conjugation. In both groups, heparin release peaked at 3 days, whereas the amount released between 3 and 7 days was negligible (<0.01%). According to these results, scaffolds used for growth factor incorporation and cell culture where washed for 3 days in ddH_2O to ensure complete removal of unbound heparin.

The proportion of heparin bound to the scaffolds after 3 days washing in ddH_2O was quantified to determine the amount of heparin available at the moment of growth factor conjugation. In non-cross-linked scaffolds, the amount of bound heparin after washing was 5.5 ± 2.1%, corresponding to a total of 0.09 ± 0.002 mg of heparin/mg of scaffold (1.6 ± 0.03 mg heparin/scaffold) (figure 2A, plain bars). In heparin-cross-linked scaffolds, the amount of bound heparin after washing was significantly higher ($p<0.001$) and averaged 26.6 ± 4%, corresponding to a total of 0.47 ± 0.02 mg of heparin/mg of scaffold (8.0 ± 0.3 mg heparin/scaffold) (figure 2A, plain bars).

3.3 Heparin functionalization did not impact growth factor incorporation, that overall resulted higher than 90%

The loading efficiency of TGF-β2 and GDF5 on biphasic scaffolds was quantified as the percentage of growth factors bound to the scaffolds with respect to the total amount of growth factors added for loading (figure 3).

For the entire scaffolds, loading efficiency of TGF-β2 averaged 94% in untreated scaffolds (without heparin), 92% in non-cross-linked scaffolds (heparin) and 96% in heparin-cross-linked scaffolds (heparin in presence of EDC/NHS) (figure 3A). Similarly, the amount of incorporated GDF5 in whole scaffolds averaged 96% in unmodified scaffolds, 92% in non-cross-linked scaffolds and 94% in heparin-cross-linked scaffolds (figure 3B). There were no statistically significant differences between groups.

Next, the growth factor loading efficiencies in the anisotropic (tendon/ligament) and isotropic (bone) regions was individually evaluated. In figures 3C and 3D, it can be observed that loading efficiency tended to be higher at the isotropic region. For TGF-β2, loading efficiency in the isotropic region averaged 98% in unmodified scaffolds, 97% in non-crosslinked scaffolds and 96% in heparin-crosslinked scaffolds (figure 3C). In the anisotropic region, TGF-β2 loading efficiency averaged 89% in untreated scaffolds, 88% in non-crosslinked scaffolds and 95% in heparin-crosslinked scaffolds (figure 3C). Both the differences between scaffold types (untreated, non-crosslinked and heparin-crosslinked) and between scaffold regions (anisotropic and isotropic) were not statistically significant. For GDF5, loading efficiency in the isotropic region averaged 97% in unmodified scaffolds, 92% in non-crosslinked scaffolds and 94% in heparin-crosslinked scaffolds (figure 3D). In the anisotropic region, GDF5 loading efficiency averaged 90% in untreated scaffolds, 75% in non-crosslinked scaffolds and 91% in heparin-crosslinked scaffolds (figure 3D). In non-crosslinked scaffolds, GDF5 incorporation was significantly higher in the isotropic compared to the anisotropic regions ($p<0.05$). On the other

hand, there were no statistically significant differences on GDF5 loading efficiency when comparing the anisotropic and isotropic parts of unmodified and heparin-crosslinked scaffolds.

3.4 Heparin functionalization increased growth factor retention on the scaffolds. Growth factors release is faster from the bony part than from the tendon/ligament part

The amount of TGF-β2 and GDF5 released from the scaffolds in cell culture medium was quantified over a period of 14 days. The amount of released growth factor was expressed as percentage relative to the amount of growth factor supplemented for loading.

When analyzing the growth factor release from whole scaffolds, the main amount of growth factors was released 24h after loading in all types of scaffolds (figures 3E and 3F). However, the patterns of growth factor release were different depending on the type of scaffold. In unmodified scaffolds or scaffolds not cross-linked with heparin, between 40 - 47% of incorporated TGF-β2 was released after 24h (figure 3E). On the other hand, only 21% of incorporated TGF-β2 was released after 24h when heparin was previously cross-linked to the scaffolds ($p<0.001$). At the end of the observation period, i.e. 14 days, 58% of incorporated TGF-β2 was released in unmodified scaffolds or scaffolds not cross-linked with heparin. Scaffold functionalization with heparin using EDC/NHS cross-linkers resulted in retardation of the TGF-β2 release to 26% (figure 3E, 14 days, $p<0.001$). GDF5 release from the scaffolds (analyzed as entire scaffold) followed a pattern similar to TGF-β2, but the differences between groups were more pronounced (figure 3F). Up to 80% GDF5 was released after 24h from unmodified scaffolds or scaffolds not cross-linked with heparin (figure 3F). In scaffolds in which heparin was previously cross-linked with EDC/NHS, GDF5 release decreased to 10% after 24h ($p<0.001$). After 14 days, up to 92% GDF5 was released from unmodified scaffolds or scaffolds not cross-linked with heparin, while heparin cross-linking decreased the amount of released GDF5 to 18% ($p<0.001$). Remarkably, the functionalization with heparin via EDC/NHS resulted in significant retardation of the release of both growth factors.

Growth factor release was also individually quantified in the anisotropic (tendon/ligament) and isotropic (bone) regions of the scaffolds (figures 3G and 3H). In general, growth factor release kinetics in the individual regions followed similar patterns to growth factor release from entire scaffolds (figures 3E to 3H). For both TGF-β2 and GDF5, the release from the anisotropic and isotropic regions was significantly higher ($p<0.01$) in unmodified and non-cross-linked scaffolds compared to the scaffolds cross-linked with heparin (figures 3G and 3H). When comparing the anisotropic and isotropic regions of each type of scaffold, there were significant differences in the amount of growth factors released. In unmodified scaffolds, total TGF-β2 released at 14 days was 74% at the isotropic part and 64% at the anisotropic part ($p<0.05$) (figure 3G). Similarly, in non-crosslinked scaffolds, total TGF-β2 released at 14 days was 65% from the isotropic part and 59% from the anisotropic part ($p<0.05$). In scaffolds cross-linked with heparin, TGF-β2 release at 14 days was slightly higher at the isotropic region (29%) compared to the anisotropic region (26%), but differences were not statistically significant. GDF5 release from unmodified scaffolds was faster in the isotropic compared to the anisotropic parts. After 24h, 73% GDF5 was released from the isotropic part of unmodified scaffolds compared to 66% from the anisotropic part (figure 3H). However, total release at 14 days was not significantly different in the isotropic (79%) compared to the anisotropic (76%) regions. In scaffolds non-cross-linked with heparin, GDF5 release at 14 days was significantly higher at the isotropic region (92%) compared to the anisotropic region (85%) ($p<0.05$). In scaffolds crosslinked with heparin, 27% GDF5 was released from the isotropic region and 19% from the anisotropic region at 14 days. Differences were not statistically significant.

Overall, the release of both growth factors tended to be faster from the isotropic (bone) part compared to the anisotropic (tendon/ligament) part.

3.5 Heparin functionalization and growth factor incorporation on the scaffolds did not influence cell seeding or metabolic activity of AdMSCs

The effect of heparin and/or growth factor incorporation on cell seeding efficiency was evaluated 24h after seeding on scaffolds. Seeding efficiency was calculated as the percentage metabolic activity of cells attached to the scaffold respect to the metabolic activity of total cells seeded. AdMSCs seeding efficiency oscillated around 80% in all types of biphasic scaffolds, independently of heparin cross-linking and/or growth factor incorporation (figure 4A). There were no statistically significant differences between groups.

The effect of heparin and/or growth factor incorporation on AdMSCs metabolic activity was evaluated over a period of 7 days (figure 4B). The metabolic activity of AdMSCs on unmodified scaffolds, i.e. without heparin or growth factors is presented as dashed line for comparison. After 1 day of culture, the metabolic activity of AdMSCs growing on all scaffolds analyzed was comparable. Noteworthy, AdMSCs seeded on scaffolds with heparin cross-linking and on scaffolds loaded with TGF-β2 showed less metabolic activity. Nevertheless, no statistical significance was found between the groups. On the other hand, after 3 days of culture, the metabolic activity of AdMSCs clearly increased in all scaffolds although no statistical significance was found. At the end of the observation period, the metabolic activity of the cells slightly decreased when compared to day 3 of culture. This was not observed for the cells seeded on heparin cross-linked scaffolds for which metabolic activity remained consistent. This decrease was more noticeable for AdMSCs seeded on scaffolds loaded with TGF-β2. No statistical differences were obtained between the groups.

3.6 Incorporation of TGF-β2 favors correct gene expression in the tendon/ligament part, while the combination of TGF-β2/GDF5 enhances gene expression suitable for regeneration of the bony part and the interphase

Growth factor incorporation on scaffolds impacted the gene expression of tendon/ligament, enthesis and cartilage markers on AdMSCs. The effects of growth factors on gene expression varied depending on scaffold region (anisotropic, transition or isotropic).

The highest increase in scx expression (4-fold upregulation) was observed in the isotropic (bone) part of scaffolds loaded with TGF-β2 + GDF5 after 7 days (figure 5A). Scaffolds loaded with GDF5 alone showed similar levels of scx expression as unloaded scaffolds in all scaffold regions. In scaffolds loaded with TGF-β2 alone, scx expression levels tended to be either downregulated or similar to unloaded scaffolds. Overall, growth factor incorporation did not have any statistically significant effects on scx expression.

The effects of growth factor incorporation on collagen I expression markedly changed over time. Collagen I expression levels at 7 days were similar or lower than those of unloaded scaffolds, whereas after 14 days collagen I was upregulated in growth factor-loaded compared to unloaded scaffolds (figure 5B). In particular, collagen I expression was the highest in the anisotropic (tendon/ligament) part of scaffolds loaded with TGF-β2 at 14 days. In addition, collagen I expression was significantly upregulated in the anisotropic (tendon/ligament) and transition (enthesis) parts of scaffolds loaded with TGF-β2 + GDF5 compared to their isotropic (bone) part at 7 days ($p<0.05$). On the other hand, collagen I expression was significantly downregulated in the transition region of scaffolds loaded with GDF5 compared to the same region in unloaded scaffolds ($p<0.05$).

The expression pattern of mohawk is comparable to that of collagen I (figure 5C). After 7 days of culture, mohawk expression in growth factor-loaded scaffolds appeared to be either downregulated or similar to unloaded scaffolds. After 14 days of culture, mohawk expression was 3-fold upregulated in the anisotropic (tendon/ligament) part of scaffolds loaded with TGF-β2 and 6-fold upregulated in the transition (enthesis) part of scaffolds loaded with TGF-β2 + GDF5. However, these differences were not statistically significant.

The expression pattern of tenascin C also matched that of collagen I and mohawk (figure 5D). After 7 days, tenascin C expression levels tended to be similar or lower in growth factor-loaded scaffolds in comparison to unloaded scaffolds. In particular, tenascin C expression was significantly downregulated in the anisotropic (tendon/ligament) region of scaffolds loaded with TGF-β2 + GDF5 compared to the same region in unloaded scaffolds ($p<0.05$). Interestingly, 14 days after culture, tenascin C expression tended to be upregulated in the anisotropic (tendon/ligament) compared to the transition (enthesis) and isotropic (bone) parts of scaffolds loaded with growth factors. Differences were statistically significant only in scaffolds loaded with TGF-β2 + GDF5 ($p<0.05$)

Sox9 expression was similar in all conditions after 7 days of culture (figure 5E). The highest upregulation (2-3 fold) was observed in the isotropic (bone) part of scaffolds loaded with TGF-β2 + GDF5 although no statistical significance was obtained. After 14 days, sox9 was significantly upregulated in the transition (enthesis) region of scaffolds loaded with TGF-β2 + GDF5 ($p<0.05$). Noteworthy, an upregulation of sox9 was also observed in the anisotropic (tendon/ligament) part of scaffolds loaded with either TGF-β2 alone or TGF-β2 + GDF5 combination. However, these differences were not statistically significant.

Collagen II expression at 7 days was similar in unloaded compared to growth factor-loaded scaffolds (figure 5F). At 14 days, collagen II was significantly upregulated ($p<0.05$) in the anisotropic (tendon/ligament) part of scaffolds loaded with TGF-β2 + GDF5 compared to the same region in unloaded scaffolds. Interestingly, collagen II was also upregulated (around 3-fold) in the same region (anisotropic) of scaffolds containing GDF5 ($p>0.05$). Similar upregulation was observed for the transition (enthesis) region of TGF-β2 scaffolds and the isotropic (bone) region of TGF-β2 + GDF5 scaffolds when compared to unloaded scaffolds. However, these differences were not statistically significant.

Aggrecan expression was significantly upregulated in the isotropic (bone) part compared to the anisotropic (tendon/ligament) region of scaffolds loaded with growth factors at 7 days after culture (figure 5G, $p<0.05$ for TGF-β2 and TGF-β2 + GDF5 whereas $p>0.05$ for GDF5). Interestingly, aggrecan was significantly downregulated in the anisotropic (tendon/ligament) part of scaffolds loaded with TGF-β2 + GDF5 compared to the same region in unloaded scaffolds ($p<0.05$). After 14 days of culture, the expression of aggrecan notably increased for this scaffold region (TGF-β2 + GDF5 loaded, anisotropic), although differences are not statistically significant. This tendency of increment on aggrecan expression for the anisotropic (tendon/ligament) regions was observed for all scaffolds loaded with growth factors at this time of observation ($p>0.05$).

Collagen III expression followed a similar pattern to collagen I. At 7 days, collagen III expression was downregulated in all scaffolds containing growth factors compared to unloaded scaffolds (figure 5H). These differences were statistically significant in the transition (enthesis) part of scaffolds loaded with TGF-β2 ($p<0.05$) and in all parts of scaffolds loaded with TGF-β2 + GDF5 ($p<0.05$, $p<0.01$). On the contrary, after 14 days of culture collagen III expression tended to be upregulated in growth factor-loaded compared to unloaded scaffolds. The highest increase in gene expression was observed for the TGF-β2 + GDF5 group, in which collagen III was upregulated in all scaffold regions. In scaffolds containing TGF-β2, collagen III expression was upregulated in the anisotropic (tendon/ligament) and transition (enthesis) regions, while in scaffolds containing GDF5 it was only upregulated in the anisotropic (tendon/ligament) region. No statistical significance was obtained for any of the comparisons performed at 14 days of culture.

3.7 TGF-β2 increases collagen type I deposition in the bony and tendon/ligament part. In the tendon/ligament part and interphase, collagen type II deposition is enhanced by GDF5 alone and collagen type III deposition by TGF-β2/GDF5

The presence of collagens I, II and III was evaluated on biphasic silk fibroin scaffolds after 14 days of culture. The experimental groups analyzed were scaffolds without growth factors (heparin cross-linked, unloaded) and scaffolds loaded with TGF-β2, GDF5 or their combination. An overview of the presence of collagens type I, II and III in the anisotropic (tendon/ligament), transition (enthesis), and isotropic (bone) regions of the scaffolds is shown in figures 6, 7 and 8, respectively (left panels).

Qualitatively, collagen I appeared to be more abundant in the scaffold loaded with TGF-β2 compared to the other groups (figure 6A, left panel). Within that scaffold, collagen I staining was stronger at both ends of the anisotropic and isotropic parts compared to the inner region (core). These observations matched the semi-quantification results (figure 6B), were the area positive for collagen I in each region of the TGF-β2 scaffolds resulted significantly higher when compared to the correspondent scaffold region on the rest of analyzed groups (i.e. for the anisotropic region $p<0.0001$, for the transition $p<0.0001$ vs. unloaded and $p<0.0034$ vs. GDF5 and TGF-β2 + GDF5, and for the isotropic region $p<0.0001$). The confocal images corresponding to these groups, showed more collagen I located at the isotropic (bone) part of the scaffolds compared to the transition (enthesis) and anisotropic (tendon/ligament) parts. This observation was confirmed by the semi-quantification results illustrated in figure 6B.

Collagen II staining was more abundant in scaffolds loaded with GDF5 compared to the other groups (figure 7A, left panel). In this group, collagen II seemed more abundant in the anisotropic (tendon/ligament) and transition (enthesis) parts compared to the isotropic (bone) part. The semi-quantitative analysis partially confirmed this observation (figure 7B). Unexpectedly, the isotropic (bone) part of the unloaded scaffolds resulted in the higher area positive for collagen II ($p<0.0001$, all groups compared by ANOVA). Scaffolds loaded with TGF-β2 + GDF5 showed comparatively more collagen II staining than the unloaded and TGF-β2

groups. In these scaffolds, collagen II concentrated at the transition (enthesis) and isotropic (bone) parts of the scaffold.

Collagen III staining appeared to be the strongest in scaffolds loaded with TGF-β2 + GDF5 (figure 8A). In these scaffolds, collagen III concentrated at the anisotropic (tendon/ligament) and transition (enthesis) regions. This was confirmed by the semi-quantitative analysis, that showed significantly higher collagen III stained area for TGF-β2 + GDF5 scaffolds when compared to the rest of the analyzed groups (figure 8B; matching scaffold regions compared among them; $p<0.0001$ for anisotropic and for the transition). Interestingly, unloaded scaffolds also seemed to result in relatively high collagen III deposition. Scaffolds loaded with single growth factor, i.e. TGF-β2 or GDF5 seemed to have lower collagen III deposits compared to unloaded scaffolds and scaffolds loaded with both growth factors combined (figure 8B). Noteworthy is the negligent collagen III deposition in the anisotropic (tendon/ligament) part of the TGF-β2 loaded scaffold (figure 1B, $p<0.05$).

In all types of scaffolds, the actin cytoskeleton aligned in the direction of the scaffold's pores (figures 6A, 7A, and 8A- middle and right columns). The cell cytoskeleton appeared elongated in the anisotropic (tendon/ligament) part of the scaffolds, while there was no apparent alignment in the isotropic (bone) part.

4. Discussion and conclusions

Functional repair of soft-to-hard tissue interfaces, such as the tendon/ligament-to-bone transition (enthesis), remains a challenge in orthopedics. Tissue engineering is a potential strategy for enthesis regeneration. However, the gradual change in tissue structure, composition, mechanical properties and cell phenotype of the enthesis poses important challenges for tissue engineering.

In this study, we developed integrated tendon/ligament-to-bone constructs cultured with human AdMSCs as an *in vitro* platform to study enthesis regeneration. The constructs are biphasic silk fibroin scaffolds that mimic the gradual change of collagen molecule alignment of the native enthesis. The scaffolds are composed of two continuous regions with different pore alignment: anisotropic (tendon/ligament-like) and isotropic (bone-like). The anisotropic and isotropic regions are integrated in a transition region (enthesis-like) with mixed aligned and non-aligned porosity. The scaffold dimensions (4mm diameter x 8mm length) were optimized for *in vitro* analysis and future implantation in small animal models (e.g. rat). The transition region (enthesis-like) spans over an area of ~500-700μm, which would be suitable for scaling up to larger animal models [35].

In a recent study, we showed that pore alignment of biphasic silk fibroin scaffolds impacted cytoskeletal alignment and gene expression of AdMSCs [6]. However, structural cues alone were not enough to promote mature stem cell chondrogenesis, fibrochondrogenesis and tenogenesis/ligamentogenesis. In the present study, we added a level of complexity to our *in vitr*o model by functionalizing biphasic silk fibroin scaffolds with heparin and loading them with TGF-β2 and/or GDF5. Our hypothesis was that the combined effects of pore alignment (structural cues) and TGF-β2/GDF5 (biochemical cues) will favorably impact stem cell differentiation in the context of enthesis regeneration.

Growth factors are potent tools to influence cell behavior. However, growth factor half-lives are short when supplemented without appropriate delivery systems [11]. In the study, TGF-β2 and/or GDF5 were delivered through covalent binding to heparin-group functionalized on the silk fibroin scaffolds' surfaces. Although no differences were observed in terms of amount of growth factors incorporated on scaffolds with or without heparin functionalization, a change in the TGF-β2 and/or GDF5 release kinetics was observed. This indicated that heparin functionalization resulted in increased growth factor retention on the scaffolds, thereby reducing burst-like release. This may result in an increase of local growth factor concentrations. The use of heparin as chemical agent to immobilize growth factors into biomaterials surface has been previously reported (reviewed in [14]). A large number of growth factors bind to heparin with relatively high affinity. This makes heparin-based delivery systems very attractive [14]. In particular for biomedical applications, the reported results are encouraging. In a recent study, Lee et al. successfully incorporated GDF5 into the surface of titanium dental implants via heparin chemistry [25]. The authors reported an effective immobilization of GDF5 as well as a sustained release of the grow factor from the heparin functionalized titanium surface. Jha et al. did report an increase of TGF-β1 immobilization on hyaluronic acid matrices that resulted proportional to the heparin concentration used [13]. The authors concluded that heparin functionalization favored both the loading and the retention of TGF-β1 into the developed hyaluronic acid materials.

Furthermore, our results are in line with those of Lee et al. that reported a GDF5 release of around 30% from heparin functionalize titanium materials after 14 days [25]. A similar behavior was also observed by Manning et al. [36] when evaluating the PDGF release from heparin/fibrin nanofibrous scaffold. The authors reported that 22% of the loaded growth factor was released during the first days of observation, and the growth factor retention was increased by the use of heparin. Our results, supported by published data, indicate that a high

proportion of growth factors remained bound to the heparin functionalized scaffold matrix, and thus a retardation on the release is obtained.

In unmodified scaffolds, growth factors bound to scaffolds through electrostatic interactions. The weak electrostatic interactions of TGF- β2 (isoelectric point (pI)= 8.82) and GDF5 (pI = 9.82) with negatively charged fibroin scaffolds resulted in burst release behavior. In an illustrative study, bovine serum albumin (BSA) (pI = 5.8) released significantly faster than VEGF (pI = 8.5), which released significantly faster than BMP-2 (pI = 8.5-9.2) from negatively charged hyaluronic acid hydrogels [37]. Burst release profile of growth factors was also observed in scaffolds functionalized with non-crosslinked heparin. This is most likely due to the dissociation of the heparin-growth factors complexes from the fibroin surfaces, due to the weak interactions between negatively charged non-crosslinked heparin (non-activated carboxyl group) and fibroin [16].

Further in vitro evaluation of scaffolds was performed using the cross-linked heparin scaffolds. The functionalization of fibroin scaffolds with cross-linked heparin with or without growth factors did not affect the cell seeding efficiency and were non-cytotoxic to AdMSCs. Similar results were reported on cell viability and proliferation of diverse cell types seeded on TGF-β1 and GDF5 loaded biomaterials via heparin conjugation [13, 25].

To further evaluate the potential of our engineered scaffolds for local delivery of TGF-β2 and GDF5 to promote enthesis regeneration, the AdMSCs differentiation and ECM productions towards the enthesis phenotype was evaluated by gene expression and collagen deposition. Scaffolds were cultured as a whole; however, evaluation was additionally also performed after separation of the scaffolds into three compartments (isotropic, interphase, and anisotropic) to enable the evaluation of cell responses in the different regions of the scaffolds, corresponding to the different internal architecture. Indeed, from gene expression, collagen I, II and III

deposition patterns to cell morphology observation, cells responses differently in each scaffold compartment.

In the anisotropic part (tendon/ligament region), single TGF-β2/GDF5 supplementation did not enhance scx (master transcription factor for tenogenesis/ ligamentogenesis [38]) expression. Similar results were obtained by Caliari et al. [4], who did not observe any effect on scx upregulation between scaffold anisotropy and 100ng/ml GDF5/7 in human bone marrow-derived mesenchymal stem cells (BM-MSCs). Notably, in the presence of TGF-β2, collagen I (most abundant extracellular matrix protein in tendons and ligaments [39]), mohawk (a critical regulator of tendon development [40]) and tenascin C (extracellular matrix protein present in tendon/ligament and enthesis [41]) were upregulated in the tendon part. This corresponded with the observation of the highest abundance of collagen I protein in the anisotropy region of scaffolds loaded with TGF-β2 compared to all other groups.

In the isotropic part (bony region), gene expression results indicated osteogenesis by way of endochondral ossification, whereby human MSCs can recapitulate endochondral ossification to form mature bone [42]. Among all the conditions evaluated in this study, just after 7 days, TGF-β2 + GDF5 enhanced sox9 (early marker for chondrogenic differentiation [43]), collagen II (most abundant type of collagen in articular cartilage [43]) and aggrecan (an abundant GAG in articular cartilage and is commonly used as a marker for cartilage ECM [43]) expression in AdMSCs while maintaining lower levels of collagen I and mohawk. Collagen II has a similar amount on protein level at the isotropic region for both GDF5 and TGF-β2 + GDF5 loaded scaffolds. Notably, abundance of collagen II protein was presence in the anisotropic region of GDF5 loaded scaffolds compared to that of TGF-β2 + GDF5 loaded scaffolds. This indicated that GDF5 promoted collagen II production [32]. However, when loaded together with TGF-β2, the effect was restricted to the interphase and isotropic region of the scaffolds. The molecular mechanism behind the synergistic effect of TGF-β2 and GDF5 in regulating the spatial

production of collagen II is not known. We stipulate that the topological cues of the scaffolds may have contributed towards the spatial expression of collagen II in the TGF-β2 + GDF5 loaded scaffolds, as the collagen II protein spatial expression is very similar to that of unloaded scaffolds. This indicated that in addition to the growth factors, the scaffold's internal architecture (e.g. pore shape, size) synergistically provides topological cues to direct AdMSCs activities [6].

The interphase of the scaffold represents the enthesis fibrocartilage region, which is still poorly understood to date. However, it has been shown that scx and sox9 are important for fibrocartilage development [44, 45]. Other fibrocartilage markers are the extracellular matrix proteins collagen II, collagen III and tenascin C and the GAG aggrecan [33, 41]. The combination of TGF-β2 + GDF5 enhanced the expression of sox9, collagen III and aggrecan in the interphase (enthesis) region of biphasic silk fibroin scaffolds. These results are supported by elevated collagen III staining at the interphase region of scaffolds loaded with TGF-β2 + GDF5 compared to all other groups.

In conclusion, our study provides new insights in the combinational effects of scaffold internal architecture and growth factors (i.e. TGF-β2 and/or GDF5) on regulation of AdMSC behaviors towards enthesis regeneration. The scaffolds' manufacturing technique coupled with activated heparin-functionalization for growth factor delivery represent a viable method for sustained and local delivery of therapeutic agents to facilitates enthesis regeneration. Indeed, TGF-β2 and GDF5 can direct AdMSCs towards the desired phenotypes for enthesis regeneration. Future improvement to our current engineered enthesis scaffolds should include spatial positioning of growth factors at designated regions and better control over the temporal release of growth factors.

The combination of highly porous lamellar-like structure with TGF-β2 loading resulted in upregulation of tendon/ligament markers. Interestingly, the addition of GDF5 to this construct

favored the expression of cartilage markers while enhancing the expression of the enthesis marker sox9 at the interface region of the biphasic scaffolds.

Limitations of our study include the lack of cell proliferation analysis over time (including long time of observation). In addition, it cannot be concluded from this study if the observed effects on gene expression are a consequence of heparin-bound or released growth factor. Future studies may benefit from comparing the effects of soluble vs. surface-bound growth factors. Further studies are needed to demonstrate the efficacy of the developed growth factor loaded biphasic silk fibroin scaffolds *in vivo* in a model of tendon/ligament-to-bone enthesis repair.

Acknowledgements

This work was supported by a grant from the Zeidler foundation "REGENTHESIS" (grant number ZFS-70), which is greatly appreciated. The authors would like to thank Carlos Peniche Silva, BSc for his valuable assistance with the semi-quantification of the confocal images.

Disclosures

Conflicts of interest: none.

References

[1] S. Font Tellado, E.R. Balmayor, M. Van Griensven, Strategies to engineer tendon/ligament-to-bone interface: Biomaterials, cells and growth factors, Advanced drug delivery reviews 94 (2015) 126-40.
[2] K.L. Moffat, W.H. Sun, P.E. Pena, N.O. Chahine, S.B. Doty, G.A. Ateshian, C.T. Hung, H.H. Lu, Characterization of the structure-function relationship at the ligament-to-bone interface, Proceedings of the National Academy of Sciences of the United States of America 105(23) (2008) 7947-52.
[3] D. Qu, C.Z. Mosher, M.K. Boushell, H.H. Lu, Engineering complex orthopaedic tissues via strategic biomimicry, Annals of biomedical engineering 43(3) (2015) 697-717.
[4] S.R. Caliari, B.A. Harley, Structural and biochemical modification of a collagen scaffold to selectively enhance MSC tenogenic, chondrogenic, and osteogenic differentiation, Advanced healthcare materials 3(7) (2014) 1086-96.
[5] L.C. Mozdzen, S.D. Thorpe, H.R. Screen, B.A. Harley, The Effect of Gradations in Mineral Content, Matrix Alignment, and Applied Strain on Human Mesenchymal Stem Cell Morphology within Collagen Biomaterials, Advanced healthcare materials 5(14) (2016) 1731-9.

[6] S. Font Tellado, W. Bonani, E.R. Balmayor, P. Foehr, A. Motta, C. Migliaresi, M. van Griensven, Fabrication and Characterization of Biphasic Silk Fibroin Scaffolds for Tendon/Ligament-to-Bone Tissue Engineering, Tissue engineering. Part A 23(15-16) (2017) 859-872.
[7] A. Motta, D. Maniglio, C. Migliaresi, H.J. Kim, X. Wan, X. Hu, D.L. Kaplan, Silk fibroin processing and thrombogenic responses, Journal of biomaterials science. Polymer edition 20(13) (2009) 1875-97.
[8] V.E. Santo, M.E. Gomes, J.F. Mano, R.L. Reis, Controlled release strategies for bone, cartilage, and osteochondral engineering--Part I: recapitulation of native tissue healing and variables for the design of delivery systems, Tissue engineering. Part B, Reviews 19(4) (2013) 308-26.
[9] A.C. Mitchell, P.S. Briquez, J.A. Hubbell, J.R. Cochran, Engineering growth factors for regenerative medicine applications, Acta biomaterialia 30 (2016) 1-12.
[10] C. Silva, A. Carretero, D. Soares da Costa, R.L. Reis, R. Novoa-Carballal, I. Pashkuleva, Design of protein delivery systems by mimicking extracellular mechanisms for protection of growth factors, Acta biomaterialia EPub ahead of print (2017).
[11] E.R. Balmayor, Targeted delivery as key for the success of small osteoinductive molecules, Advanced drug delivery reviews 94 (2015) 13-27.
[12] G. Lammers, E.M. van de Westerlo, E.M. Versteeg, T.H. van Kuppevelt, W.F. Daamen, A comparison of seven methods to analyze heparin in biomaterials: quantification, location, and anticoagulant activity, Tissue engineering. Part C, Methods 17(6) (2011) 669-76.
[13] A.K. Jha, A. Mathur, F.L. Svedlund, J. Ye, Y. Yeghiazarians, K.E. Healy, Molecular weight and concentration of heparin in hyaluronic acid-based matrices modulates growth factor retention kinetics and stem cell fate, Journal of controlled release : official journal of the Controlled Release Society 209 (2015) 308-16.
[14] S.E. Sakiyama-Elbert, Incorporation of heparin into biomaterials, Acta biomaterialia 10(4) (2014) 1581-1587.
[15] N.L. Leong, A. Arshi, N. Kabir, A. Nazemi, F.A. Petrigliano, B.M. Wu, D.R. McAllister, In vitro and in vivo evaluation of heparin mediated growth factor release from tissue-engineered constructs for anterior cruciate ligament reconstruction, Journal of orthopaedic research : official publication of the Orthopaedic Research Society 33(2) (2015) 229-36.
[16] C.C. Rider, B. Mulloy, Heparin, Heparan Sulphate and the TGF-beta Cytokine Superfamily, Molecules (Basel, Switzerland) 22(5) (2017) 713-724.
[17] T.A. McCaffrey, D.J. Falcone, C.F. Brayton, L.A. Agarwal, F.G. Welt, B.B. Weksler, Transforming growth factor-beta activity is potentiated by heparin via dissociation of the transforming growth factor-beta/alpha 2-macroglobulin inactive complex, The Journal of cell biology 109(1) (1989) 441-8.
[18] J. Ratanavaraporn, Y. Tabata, Enhanced osteogenic activity of bone morphogenetic protein-2 by 2-O-desulfated heparin, Acta biomaterialia 8(1) (2012) 173-182.
[19] S.T. Nillesen, P.J. Geutjes, R. Wismans, J. Schalkwijk, W.F. Daamen, T.H. van Kuppevelt, Increased angiogenesis and blood vessel maturation in acellular collagen-heparin scaffolds containing both FGF2 and VEGF, Biomaterials 28(6) (2007) 1123-31.
[20] K.H. Koo, J.M. Lee, J.M. Ahn, B.S. Kim, W.G. La, C.S. Kim, G.I. Im, Controlled delivery of low-dose bone morphogenetic protein-2 using heparin-conjugated fibrin in the posterolateral lumbar fusion of rabbits, Artificial organs 37(5) (2013) 487-94.
[21] O. Jeon, S.J. Song, S.W. Kang, A.J. Putnam, B.S. Kim, Enhancement of ectopic bone formation by bone morphogenetic protein-2 released from a heparin-conjugated poly(L-lactic-co-glycolic acid) scaffold, Biomaterials 28(17) (2007) 2763-71.
[22] F.P. Seib, M. Herklotz, K.A. Burke, M.F. Maitz, C. Werner, D.L. Kaplan, Multifunctional silk-heparin biomaterials for vascular tissue engineering applications, Biomaterials 35(1) (2014) 83-91.

[23] A. Zieris, K. Chwalek, S. Prokoph, K.R. Levental, P.B. Welzel, U. Freudenberg, C. Werner, Dual independent delivery of pro-angiogenic growth factors from starPEG-heparin hydrogels, Journal of Controlled Release 156(1) (2011) 28-36.
[24] A. Watarai, L. Schirmer, S. Thönes, U. Freudenberg, C. Werner, J.C. Simon, U. Anderegg, TGFβ functionalized starPEG-heparin hydrogels modulate human dermal fibroblast growth and differentiation, Acta biomaterialia 25(Supplement C) (2015) 65-75.
[25] S.J. Lee, M.S. Bae, D.W. Lee, D.N. Heo, D. Lee, M. Heo, S.J. Hong, J. Kim, W.D. Kim, S.A. Park, I.K. Kwon, The use of heparin chemistry to improve dental osteogenesis associated with implants, Carbohydrate polymers 157 (2017) 1750-1758.
[26] M. Younesi, D.M. Knapik, J. Cumsky, B.O. Donmez, P. He, A. Islam, G. Learn, P. McClellan, M. Bohl, R.J. Gillespie, O. Akkus, Effects of PDGF-BB delivery from heparinized collagen sutures on the healing of lacerated chicken flexor tendon in vivo, Acta biomaterialia 63(Supplement C) (2017) 200-209.
[27] Y.I. Kim, J.S. Ryu, J.E. Yeo, Y.J. Choi, Y.S. Kim, K. Ko, Y.G. Koh, Overexpression of TGF-beta1 enhances chondrogenic differentiation and proliferation of human synovium-derived stem cells, Biochemical and biophysical research communications 450(4) (2014) 1593-9.
[28] B.T. Estes, B.O. Diekman, J.M. Gimble, F. Guilak, Isolation of adipose-derived stem cells and their induction to a chondrogenic phenotype, Nature protocols 5(7) (2010) 1294-311.
[29] B.A. Pryce, S.S. Watson, N.D. Murchison, J.A. Staverosky, N. Dunker, R. Schweitzer, Recruitment and maintenance of tendon progenitors by TGFbeta signaling are essential for tendon formation, Development (Cambridge, England) 136(8) (2009) 1351-61.
[30] E. Havis, M.A. Bonnin, J. Esteves de Lima, B. Charvet, C. Milet, D. Duprez, TGFbeta and FGF promote tendon progenitor fate and act downstream of muscle contraction to regulate tendon differentiation during chick limb development, Development (Cambridge, England) 143(20) (2016) 3839-3851.
[31] E.E. Storm, D.M. Kingsley, GDF5 coordinates bone and joint formation during digit development, Developmental biology 209(1) (1999) 11-27.
[32] B.I. Ayerst, R.A. Smith, V. Nurcombe, A.J. Day, C.L. Merry, S.M. Cool, Growth Differentiation Factor 5-Mediated Enhancement of Chondrocyte Phenotype Is Inhibited by Heparin: Implications for the Use of Heparin in the Clinic and in Tissue Engineering Applications, Tissue engineering. Part A 23(7-8) (2017) 275-292.
[33] N.A. Dyment, A.P. Breidenbach, A.G. Schwartz, R.P. Russell, L. Aschbacher-Smith, H. Liu, Y. Hagiwara, R. Jiang, S. Thomopoulos, D.L. Butler, D.W. Rowe, Gdf5 progenitors give rise to fibrocartilage cells that mineralize via hedgehog signaling to form the zonal enthesis, Developmental biology 405(1) (2015) 96-107.
[34] S. Schneider, M. Unger, M. van Griensven, E.R. Balmayor, Adipose-derived mesenchymal stem cells from liposuction and resected fat are feasible sources for regenerative medicine, European journal of medical research 22(1) (2017) 17.
[35] L. Rossetti, L.A. Kuntz, E. Kunold, J. Schock, K.W. Muller, H. Grabmayr, J. Stolberg-Stolberg, F. Pfeiffer, S.A. Sieber, R. Burgkart, A.R. Bausch, The microstructure and micromechanics of the tendon-bone insertion, Nature materials 16(6) (2017) 664-670.
[36] C.N. Manning, A.G. Schwartz, W. Liu, J. Xie, N. Havlioglu, S.E. Sakiyama-Elbert, M.J. Silva, Y. Xia, R.H. Gelberman, S. Thomopoulos, Controlled delivery of mesenchymal stem cells and growth factors using a nanofiber scaffold for tendon repair, Acta biomaterialia 9(6) (2013) 6905-14.
[37] J. Patterson, R. Siew, S.W. Herring, A.S. Lin, R. Guldberg, P.S. Stayton, Hyaluronic acid hydrogels with controlled degradation properties for oriented bone regeneration, Biomaterials 31(26) (2010) 6772-81.
[38] H. Liu, S. Zhu, C. Zhang, P. Lu, J. Hu, Z. Yin, Y. Ma, X. Chen, H. OuYang, Crucial transcription factors in tendon development and differentiation: their potential for tendon regeneration, Cell and tissue research 356(2) (2014) 287-98.

[39] A. Subramanian, T.F. Schilling, Tendon development and musculoskeletal assembly: emerging roles for the extracellular matrix, Development (Cambridge, England) 142(24) (2015) 4191-204.
[40] Y. Ito, N. Toriuchi, T. Yoshitaka, H. Ueno-Kudoh, T. Sato, S. Yokoyama, K. Nishida, T. Akimoto, M. Takahashi, S. Miyaki, H. Asahara, The Mohawk homeobox gene is a critical regulator of tendon differentiation, Proceedings of the National Academy of Sciences of the United States of America 107(23) (2010) 10538-42.
[41] C.F. Liu, L. Aschbacher-Smith, N.J. Barthelery, N. Dyment, D. Butler, C. Wylie, Spatial and temporal expression of molecular markers and cell signals during normal development of the mouse patellar tendon, Tissue engineering. Part A 18(5-6) (2012) 598-608.
[42] C. Scotti, E. Piccinini, H. Takizawa, A. Todorov, P. Bourgine, A. Papadimitropoulos, A. Barbero, M.G. Manz, I. Martin, Engineering of a functional bone organ through endochondral ossification, Proceedings of the National Academy of Sciences of the United States of America 110(10) (2013) 3997-4002.
[43] L. Quintana, N.I. zur Nieden, C.E. Semino, Morphogenetic and regulatory mechanisms during developmental chondrogenesis: new paradigms for cartilage tissue engineering, Tissue engineering. Part B, Reviews 15(1) (2009) 29-41.
[44] J. Baek, X. Chen, S. Sovani, S. Jin, S.P. Grogan, D.D. D'Lima, Meniscus tissue engineering using a novel combination of electrospun scaffolds and human meniscus cells embedded within an extracellular matrix hydrogel, Journal of orthopaedic research : official publication of the Orthopaedic Research Society 33(4) (2015) 572-83.
[45] E. Blitz, S. Viukov, A. Sharir, Y. Shwartz, J.L. Galloway, B.A. Pryce, R.L. Johnson, C.J. Tabin, R. Schweitzer, E. Zelzer, Bone ridge patterning during musculoskeletal assembly is mediated through SCX regulation of Bmp4 at the tendon-skeleton junction, Developmental cell 17(6) (2009) 861-73.

Statement of significance

Regeneration of the tendon/ligament-to-bone interface (enthesis) is of significance in the repair of ruptured tendons/ligaments to bone to improve implant integration and clinical outcome. This study proposes a novel approach for enthesis regeneration based on a biomimetic and integrated tendon/ligament-to-bone construct, stem cells and heparin-based delivery of growth factors. We show that heparin can keep growth factors local and biologically active at low doses, which is critical to avoid supraphysiological doses and associated side effects. In addition, we identify synergistic effects of biological (growth factors) and structural (pore alignment) cues on stem cells. These results improve current understanding on the combined impact of biological and structural cues on the multi-lineage differentiation capacity of stem cells for regenerating complex tissue interfaces.

Graphical Abstract

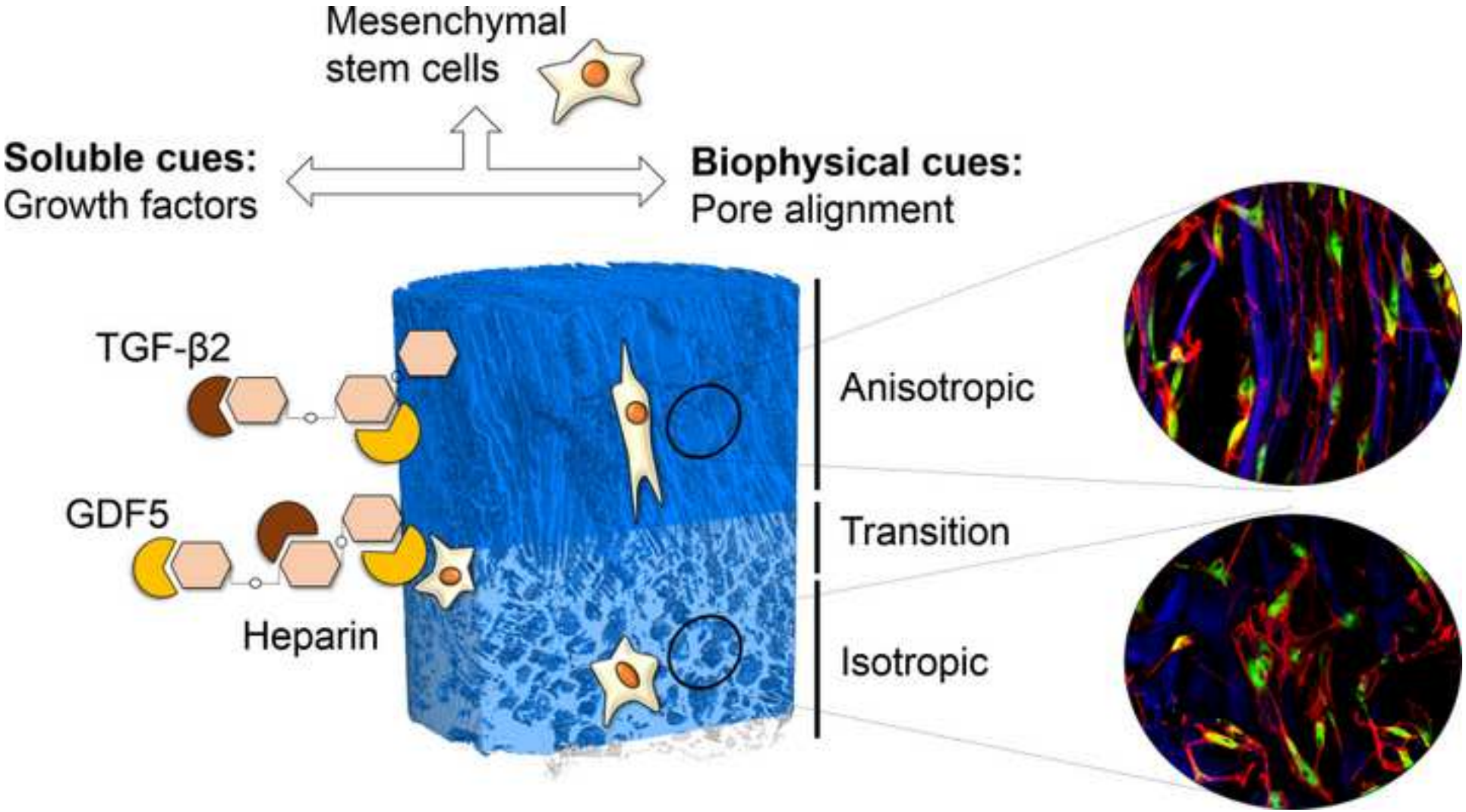

Figure captions

Figure 1. Morphological characterization of biphasic silk fibroin scaffolds. A) Digital light microscopy images showing transversal sections of a biphasic silk fibroin scaffold. The inner region of the scaffold is shown in the left panel, while the surface is shown in the right panel. The parts of the scaffold corresponding to the anisotropic (tendon/ligament), transition and isotropic (bone) regions are indicated by colored boxes added to the images. Scaffold dimensions are 4mm diameter x 8mm length. Scale bars = 1mm. The left panel shows the surface roughness of each region of the scaffolds. **B)** 3D reconstruction of a biphasic silk fibroin scaffold performed with micro-computed tomography. The 3D reconstruction shows a scaffold transversal section, where pore morphology and alignment can be appreciated. The anisotropic (tendon/ligament), transition and isotropic (bone) regions are indicated by colored boxes added to the image. Relevant parameters for 3D structural analysis, i.e. fractal dimension (FD), degree of anisotropic (DA) as well as **C)** porosity and pore size distribution were calculated for each region (n= 6). **D)** Scanning electron microscopy images (first and third) and fluorescence microscopy images (second and fourth, DAPI staining) showing pore morphology and alignment in the anisotropic (tendon/ligament), transition and isotropic (bone) regions of biphasic scaffolds. In the anisotropic (tendon/ligament) region, scaffold pores are aligned and have a lamellar-like morphology. In the isotropic (bone) region, pores are round and non-aligned. At the transition, the lamellar pores penetrate the round pores generating an integrated area of mixed porosity. Scale bars = 300 μm (first and third images) or 500μm (second and fourth images).

Figure 2. Heparin loading efficiency and release. A) Loading efficiency of heparin on biphasic silk fibroin scaffolds in the presence (crosslinked) or absence (non-crosslinked) of EDC/NHS. The bars indicate the amount of heparin bound to the scaffolds after conjugation (before (hatched bars) or after (solid bars) washing the scaffolds for 3 days in ddH_2O). The amount of bound heparin is expressed as percentage

relative to the amount of heparin used for conjugation (30mg/ml). n=6, mean ± SEM. Statistical significance is indicated with asterisks (***p<0.001). **B)** Cumulative release of heparin from biphasic silk fibroin scaffolds (non-crosslinked or crosslinked with heparin) after 1h, 3h, 1d, 3d and 7d of incubation in ddH_2O. The amount of released heparin is expressed as percentage with respect to the amount of heparin bound to the scaffolds after conjugation. n=6, mean ± SEM.

Figure 3. Growth factor incorporation and release. Incorporation efficiency of transforming growth factor β2 (TGF-β2) to: **A)** entire biphasic silk fibroin scaffold or **C)** to the anisotropic and isotropic regions separately. Incorporation efficiency of growth/differentiation factor 5 (GDF5) to: **B)** entire biphasic silk fibroin scaffolds or **D)** to the anisotropic and isotropic regions separately. The groups analyzed are unmodified scaffolds, scaffolds non-crosslinked with heparin or scaffolds crosslinked with heparin. Incorporation efficiency is expressed as the percentage of growth factor bound to the scaffolds of the total supplemented for loading. n=3, mean ± SEM. Cumulative release from entire biphasic silk fibroin scaffolds: **E)** TGF-β2 or **F)** GDF5. Cumulative release from the anisotropic (tendon/ligament) and isotropic (bone) regions separately: **G)** TGF-β2 or **H)** GDF5. The groups analyzed are unmodified scaffolds, scaffolds non-crosslinked with heparin or scaffolds crosslinked with heparin. Growth factor release was quantified after 1h, 3h, 1d, 3d, 7d or 14d of incubation in cell culture medium. The amount of released growth factors is expressed as percentage of the amount of growth factor supplemented for loading (100ng/scaffold). n=3, mean ± SEM. Statistical significance is indicated with asterisks. *p<0.05, **p<0.01, ***p<0.001.

Figure 4. Adipose-derived mesenchymal stem cells (AdMSCs) seeding efficiency and metabolic activity. **A)** Seeding efficiency of AdMSCs on biphasic silk fibroin scaffolds unmodified, crosslinked with heparin

without growth factors (unloaded) or crosslinked with heparin and loaded with TGF-β2, GDF5 or their combination. Seeding efficiency is expressed as percentage of metabolic activity of cells attached to the scaffolds in relation to the metabolic activity of total cells seeded. Metabolic activity was quantified 24h after seeding. N=3, n=9, mean ± SEM. **B)** Metabolic activity of AdMSCs cultured on biphasic silk fibroin scaffolds crosslinked with heparin (unloaded or loaded with TGF-β2, GDF5 or their combination) expressed as percentage of metabolic activity of AdMSCs on unmodified scaffolds (dashed line). Metabolic activity was quantified after 1, 3 or 7 days of culture. N=3, n=9, mean ± SEM.

Figure 5. Influence of scaffold pore alignment and growth factors on adipose-derived mesenchymal stem cells (AdMSCs) gene expression. Quantitative analysis of gene expression performed in AdMSCs cultured on biphasic silk fibroin scaffolds crosslinked with heparin and loaded with TGF-β2, GDF5 or their combination (7 and 14 days of culture). Target genes are scleraxis **(A)**, collagen I **(B)**, mohawk **(C)**, tenascin C **(D)**, SRY-box 9 (sox9) **(E)**, collagen II **(F)**, aggrecan **(G)** and collagen III **(H).** Housekeeper gene is β-Tubulin. Target gene expression was analyzed in each scaffold region (anisotropic (tendon/ligament), transition and isotropic(bone)) individually and expressed as $2^{-\Delta\Delta CT}$ relative to the housekeeper and to target gene expression in unloaded scaffolds (dashed line). Normalization to target gene expression in unloaded scaffolds was performed for each scaffold region individually. N=3, n=9, mean ± SEM. Statistical significance is indicated with asterisks. *p<0.05, **p<0.01. Asterisks on top of a bar indicate statistical significance respect to unloaded scaffolds.

Figure 6. Influence of scaffold pore alignment and growth factors on collagen I production. Collagen I content and AdMSCs cytoskeletal morphology was analyzed after 14 days of culture on heparin-crosslinked biphasic silk fibroin scaffolds unloaded or loaded with TGF-β2, GDF5 or their combination. **A)**

Left column: immunofluorescence staining of transversal sections of biphasic silk fibroin scaffolds (blue staining, DAPI) showing collagen I content (green staining). Scale bars = 1mm. Dashed squares represent the areas of the scaffolds where higher magnification images were taken as represented in the middle and right columns: immunofluorescence staining images of the anisotropic (tendon/ligament) and isotropic (bone) regions of the scaffolds at higher magnification. The images show scaffold pore alignment (blue staining, DAPI), AdMSCs actin cytoskeleton (red staining, Phalloidin) and collagen I (green staining). Scale bars = 200µm. **B)** Semi-quantification of the collagen I staining performed by ImageJ analysis. n=5, mean ± SD. Statistical significance is indicated with symbols. ****p<0.0001, # anisotropic p<0.0001, $ interface: p<0.0001 vs. unloaded and p<0.0034 vs. GDF5, & isotropic p<0.0001.

Figure 7. Influence of scaffold pore alignment and growth factors on collagen II production. Collagen II content and AdMSCs cytoskeletal morphology was analyzed after 14 days of culture on heparin-crosslinked biphasic silk fibroin scaffolds unloaded or loaded with TGF-β2, GDF5 or their combination. **A)** Left column: immunofluorescence staining of transversal sections of biphasic silk fibroin scaffolds (blue staining, DAPI) showing collagen II content (green staining). Scale bars = 1mm. Dashed squares represent the areas of the scaffolds where higher magnification images were taken as represented in the middle and right columns: immunofluorescence staining images of the anisotropic and isotropic regions of the scaffolds at higher magnification. The images show scaffold pore alignment (blue staining, DAPI), AdMSCs actin cytoskeleton (red staining, Phalloidin) and collagen II (green staining). Scale bars = 200µm. **B)** Semi-quantification of the collagen II staining performed by ImageJ analysis. n=5, mean ± SD. Statistical significance is indicated with symbols. ***p<0.001, ****p<0.0001, # anisotropic p<0.0001, $ interface p<0.0001, & isotropic p<0.0001.

Figure 8. Influence of scaffold pore alignment and growth factors on collagen III production. Collagen III content and AdMSCs cytoskeletal morphology was analyzed after 14 days of culture on heparin-crosslinked biphasic silk fibroin scaffolds unloaded or loaded with TGF-β2, GDF5 or their combination. **A)** Left column: immunofluorescence staining of transversal sections of biphasic silk fibroin scaffolds (blue staining, DAPI) showing collagen III content (green staining). Scale bars = 1mm. Dashed squares represent the areas of the scaffolds where higher magnification images were taken as represented in the middle and right columns: immunofluorescence staining images of the anisotropic and isotropic regions of the scaffolds at higher magnification. The images show scaffold pore alignment (blue staining, DAPI), actin cytoskeleton (red staining, Phalloidin) and collagen III (green staining). Scale bars = 200µm. **B)** Semi-quantification of the collagen III staining performed by ImageJ analysis. n=5, mean ± SD. Statistical significance is indicated with symbols. ****p<0.0001, # anisotropic p<0.0001, $ interface p<0.0001, & isotropic p<0.0001.

Figure 1 R1

Click here to download high resolution image

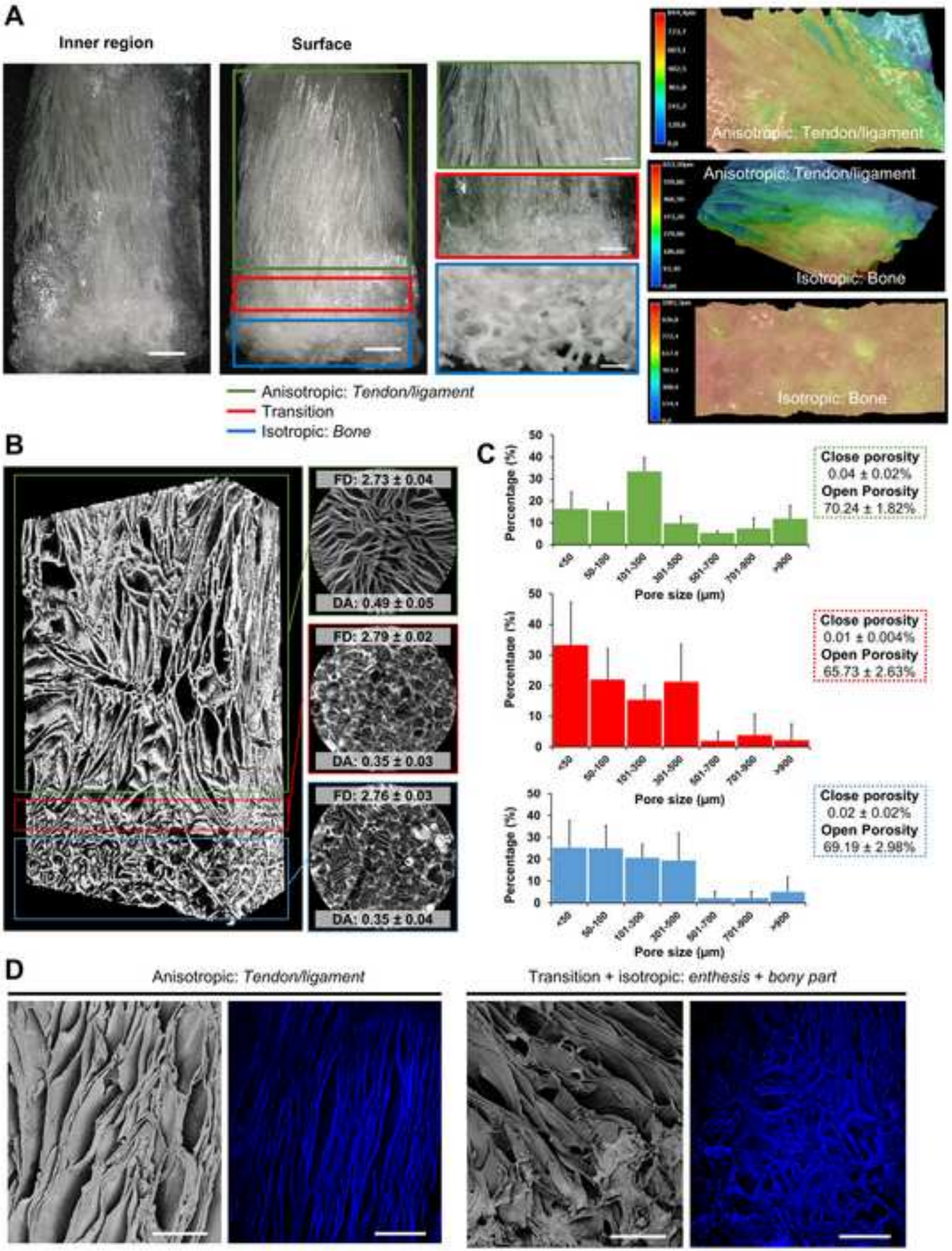

Figure 2 R1

Click here to download high resolution image

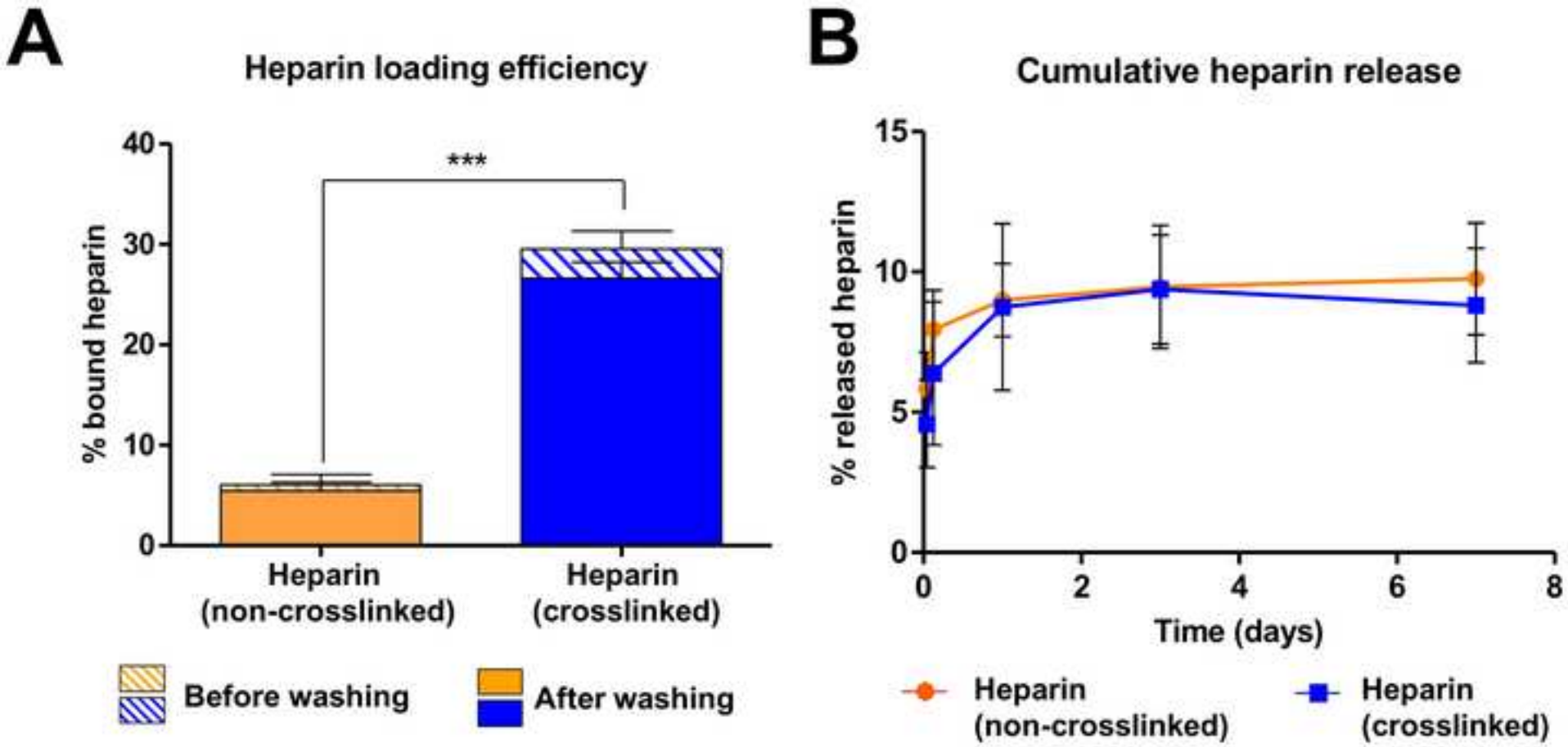

Figure 3 R1

Click here to download high resolution image

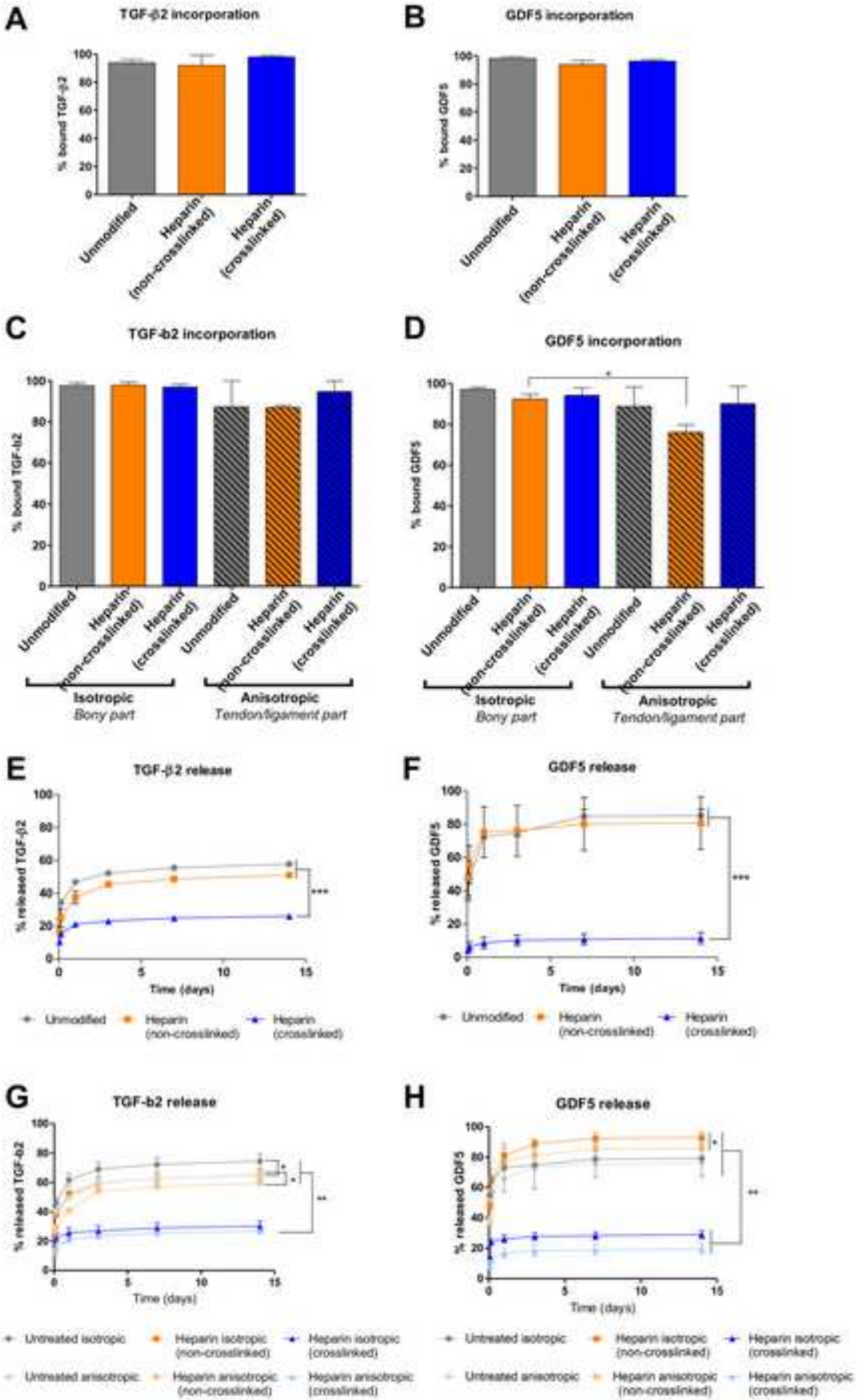

Figure 4 R1

Click here to download high resolution image

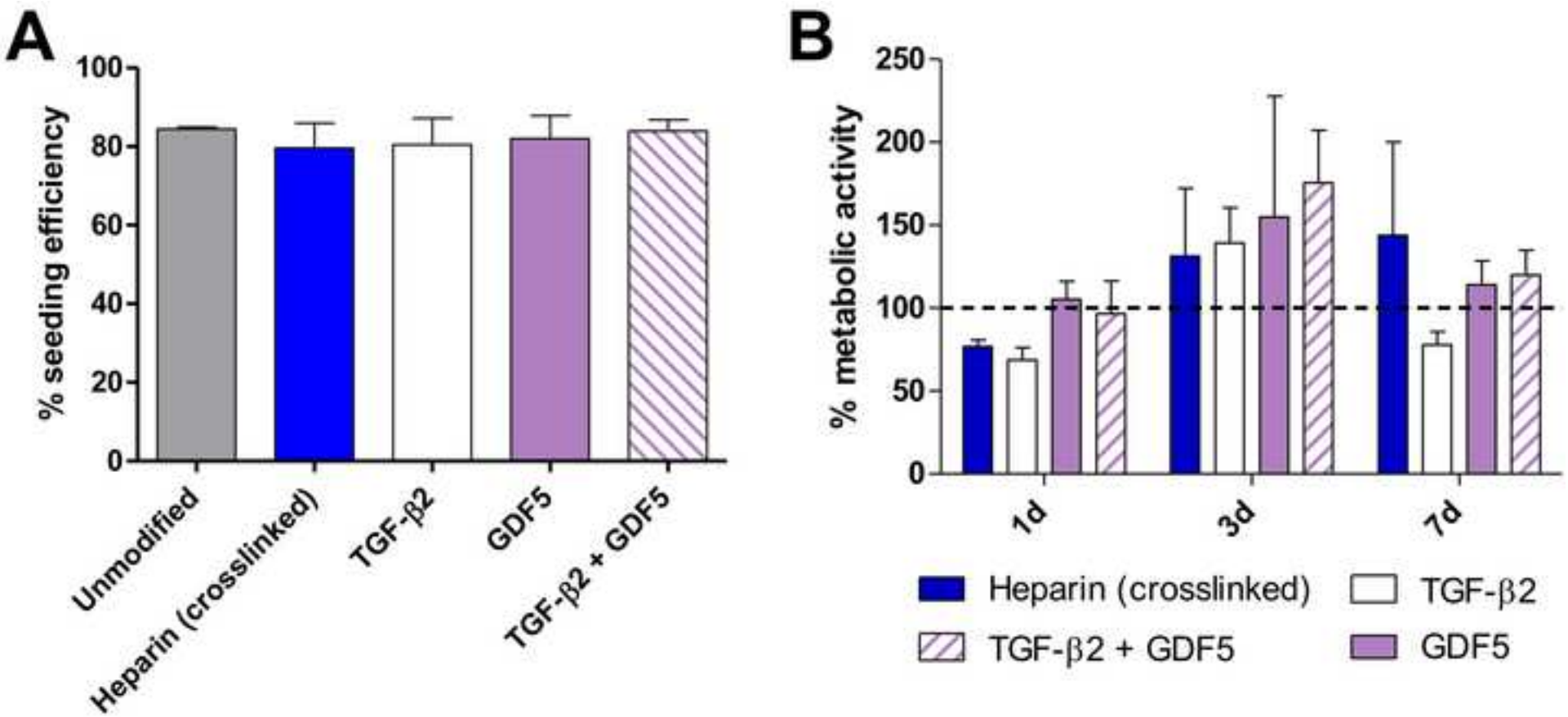

Figure 5 R1

Click here to download high resolution image

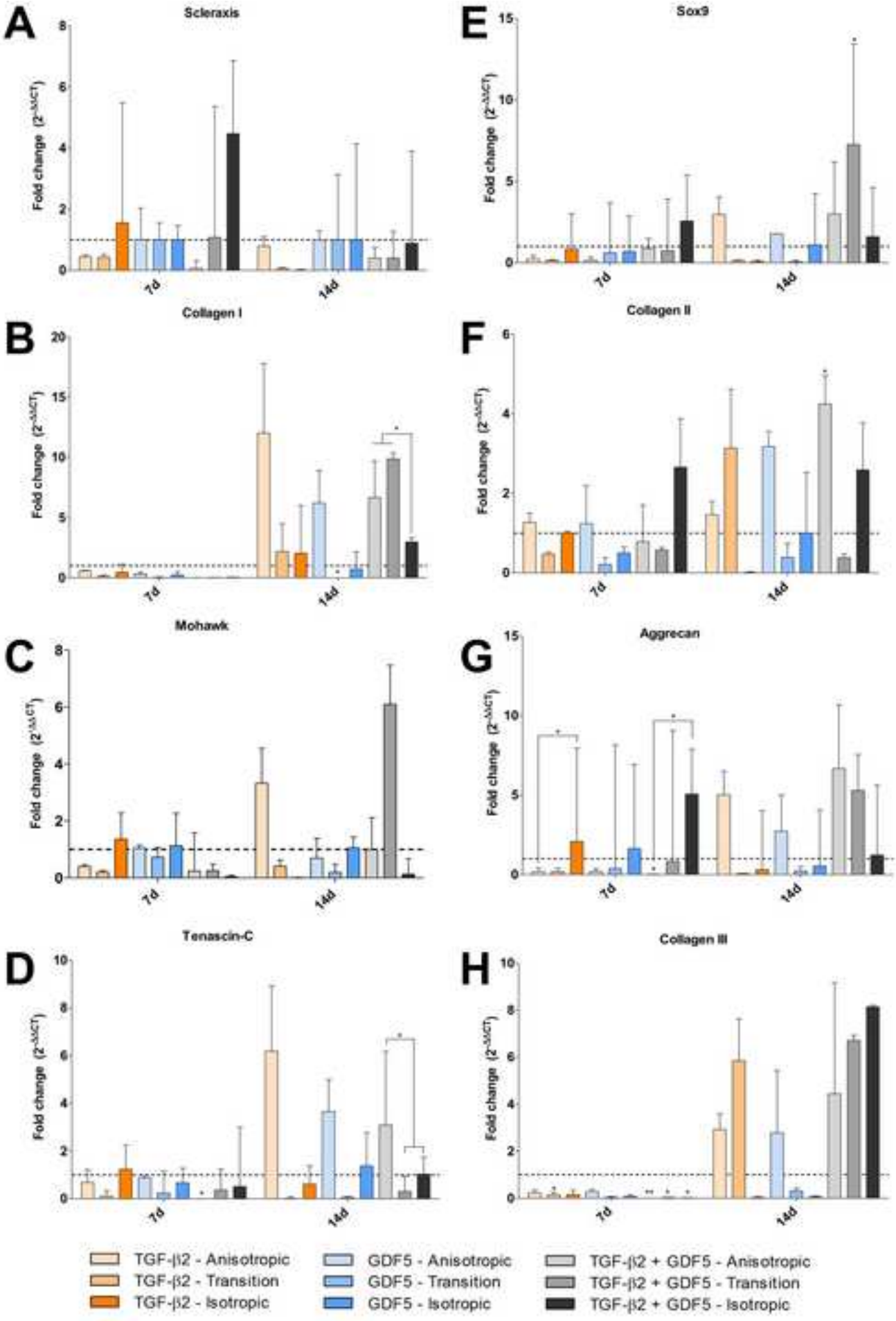

Figure 6 R1

Click here to download high resolution image

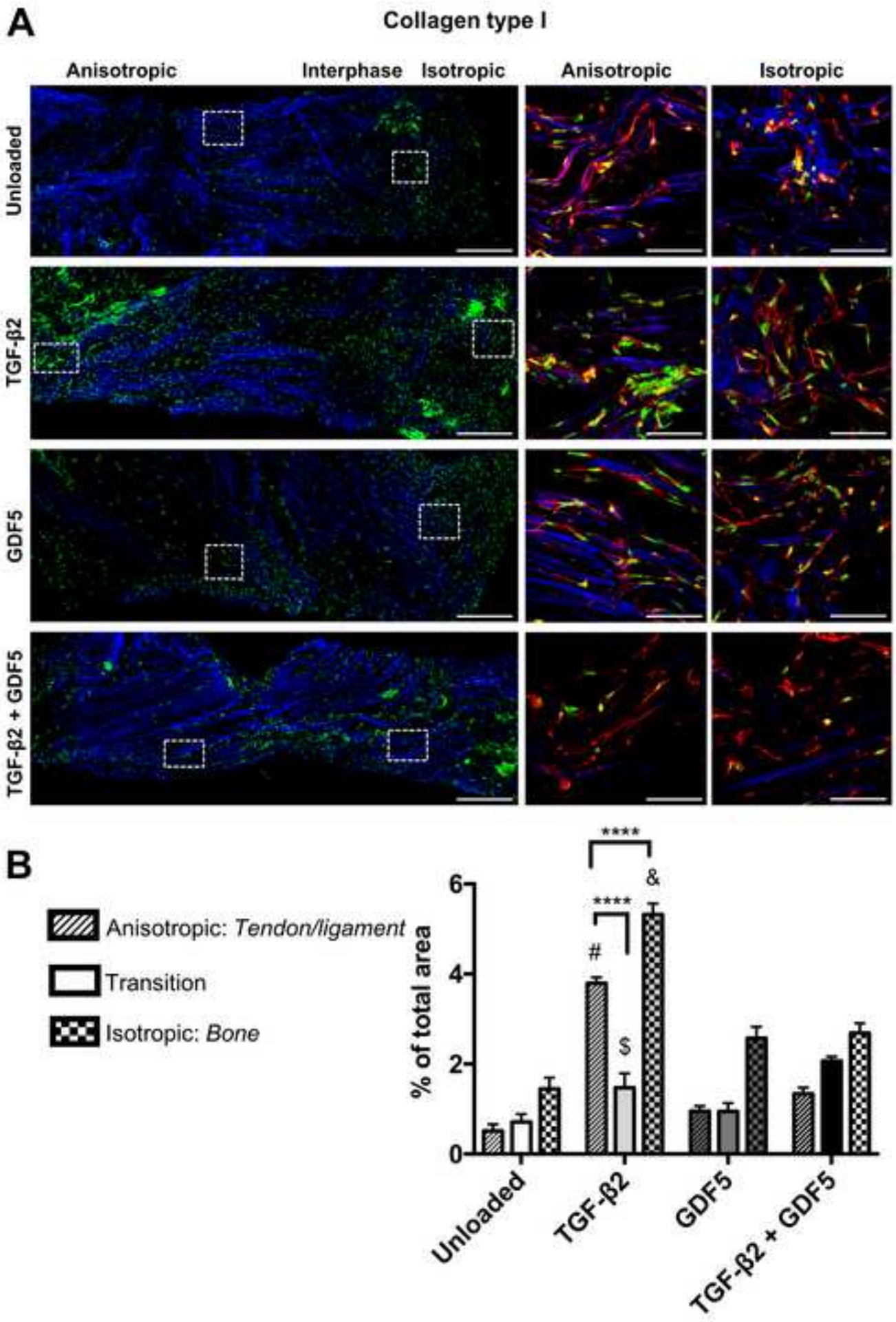

Figure 7 R1

Click here to download high resolution image

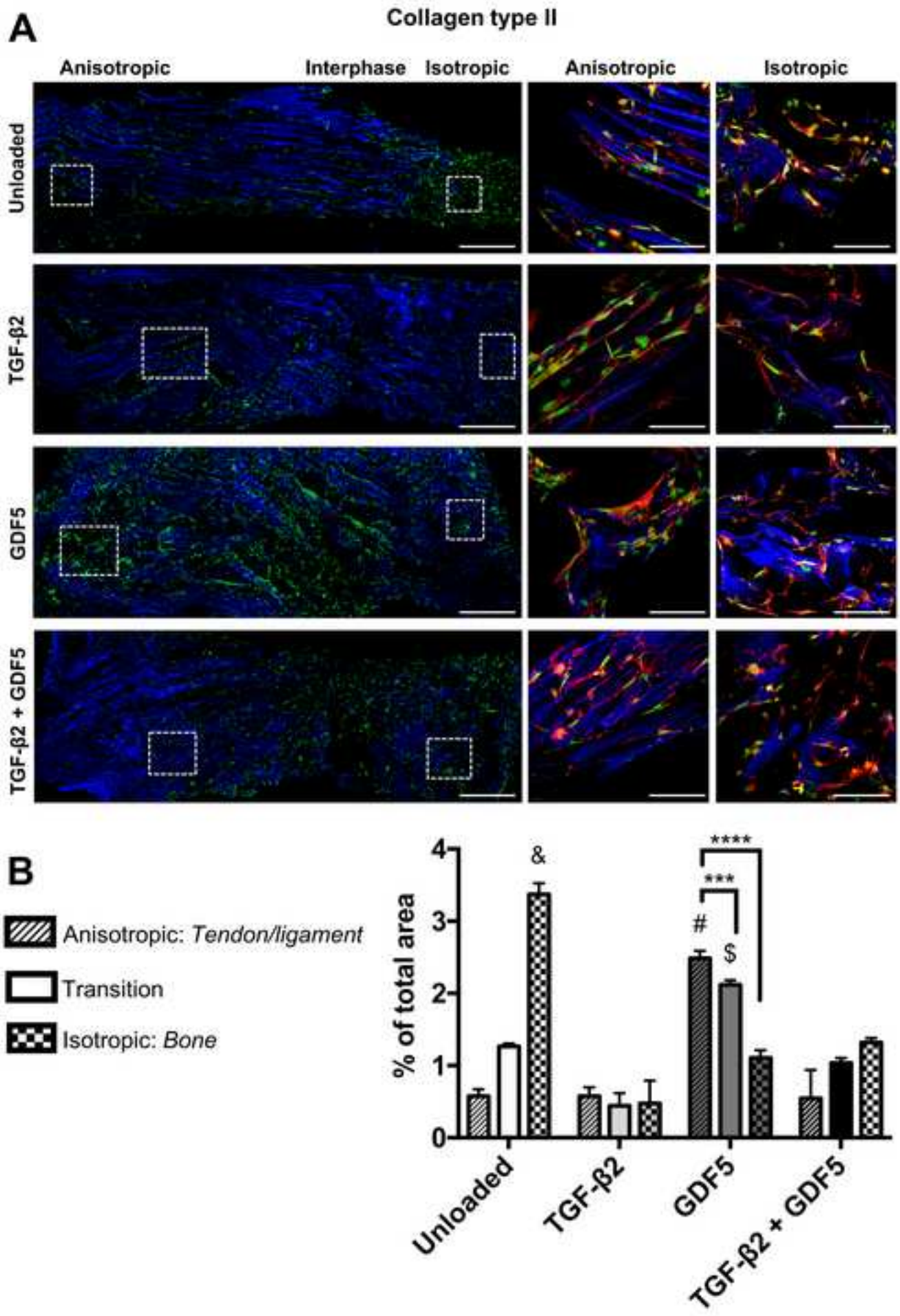

Figure 8 R1

Click here to download high resolution image